EVALUATING MACROPORE FLOW WITH TEMPORAL ELECTRICAL RESISTIVITY IMAGING IN RIPARIAN AREAS

By

JOHN PAUL HAGER

Bachelor of Science in Geology

Western Michigan University

Kalamazoo, MI

2018

Submitted to the Faculty of the
Graduate College of the
Oklahoma State University
in partial fulfillment of
the requirements for
the Degree of
MASTER OF SCIENCE
May, 2021

EVALUATING MACROPORE FLOW WITH

TEMPORAL ERI IN RIPARIAN AREAS

Thesis Approved:

Todd Halihan

Thesis Adviser

Javier Vilcaez

Ahmed Ismail

ACKNOWLEDGEMENTS

Financial support for this thesis was provided by the United States Department of Agriculture, under the branch of NIFA – the National Institute of Food and Agriculture. (Project number #2016-67019-26855).

I would like to thank Dr. Todd Halihan for facilitating a project in Balmorhea, Texas that provided field experience and financial support during my graduate studies. Thanks goes out to North Carolina State University (NCSU) – Biological and Agricultural Engineering for Dr. Garey Fox and Dr. Lucie Guertault for equipment use and assistance in conducting the experiments. This project was in collaboration with NCSU and wouldn't have been possible without their help. I would also like to thank Jordon Massey for assistance in the field and data collection. Lastly, I would love to thank my mother for continued support.

Name: JOHN PAUL HAGER

Date of Degree: MAY, 2018

Title of Study: EVALUATING MACROPORE FLOW WITH TEMPORAL ERI IN RIPARIAN AREAS

Major Field: GEOLOGY

Abstract: Riparian soils are uniquely susceptible to the formation of macropores, voids with preferential flow in comparison to surrounding strata, which are hypothesized to promote fast transport of water through soil layers. Electrical Resistivity Imaging (ERI) can locate spatial heterogeneities in soil wetting patterns caused by preferential flow through macropores, thus optimizing the design of riparian buffers. Temporal ERI (TERI) imaging was conducted in a fine and coarse field setting with artificial macropores to evaluate flow under unsaturated simulated rainfall conditions and saturated infiltrometer conditions.

Results from field data show that while macropores are detectable using TERI datasets, this results in an average field setting would detect the wetted zone in the vicinity of a macropore, not the macropore itself. The results were similar for both the primary fine grain soil site in Oklahoma as well as the coarse grain site in North Carolina. TERI data indicate that without artificial rainfall or macropores in low noise conditions, a single macropore would not be detected, a wetted zone would be the best detection. In a field evaluation of naturally occurring macropores, the TERI technique would detect the wetted zone around a macropore similar to an area of increased hydraulic conductivity in a heterogeneous soil matrix. The findings from the first set of experimentation indicate an appropriate resolution and electrode spacing for the second experiment in this thesis. The second experiment entails the tracer velocity mapping of alluvial soil. Preliminary results show TERI as a viable method for calculating the fluid velocity along a series of vertical profiles in the coarse-grained North Carolina field site.

TABLE OF CONTENTS

Chapter Page

CHAPTER I 1
CHAPTER II 3
INTRODUCTION 3
SITE DESCRIPTION 6
METHODOLOGY 8
Experimental Field Design: 8
ERI Design: 9
Wetting Approaches: 11
Imaging Experiments: 12
TERI Analysis: 13
RESULTS 14
Data Quality: 14
Single Macropore Detectability: 15
Multiple Macropores Saturated versus Unsaturated: 18
COARSE SOIL VERSUS FINE SOIL 19
DISSCUSSION 20
Can TERI Detect a Single Macropore? 21
Does TERI locate macropores precisely? 21
When Do Macropores Activate? 22
Future Work 22
CONCLUSION 23
CHAPTER III 24
introduction 24
SITE DESCRIPTION 27

METHODs 29
Wetting Methods: 30
TERI Data Collection Methods: 31
TERI Analysis: 32
RESULTS 33
Data Quality: 33
Range and Trends of Resistivity Values: 34
Range and Trends in Temporal Changes: 36
Types of Temporal Changes: 37
Hydraulic Conductivity Calculation: 41
DISCUSSION 44
Can TERI Be Utilized To Calculate Wetting Front Velocities? 44
Vertical VS Lateral Flow 45
CONCLUSION 46
REFERENCES 48

LIST OF TABLES

Table Page

Table 1 - Imaging sequence for the TERI experiments in Oklahoma and North Carolina. 13

Table 2 - Distribution of calculated hydraulic conductivities based on wetting front velocities in each vertical profile on longitudinal Line 1. The red outlined cell (4.5) represents the location of crossing with transverse Line 3. Results are shown units of in mm/hr. Figure 3.1 shows the location of TERI transects used as data sources for Tables 3.1 and 3.2. 42

Table 3 - Distribution of calculated hydraulic conductivities based on wetting front velocities in each vertical profile on transverse Line 3. The red outlined cell (6.5) represents the location of crossing with longitudinal Line 1. Results are shown in units of mm/hr. 43

LIST OF FIGURES

Figure Page

Figure 1 - Field sites for TERI experiments. A) ERI line in fine grain soil site in Oklahoma. Orange cable connects 28 stainless steel electrodes at a 1.6 meter spacing in fine soil. B) ERI line in coarse grain soil site in North Carolina. The orange cable transferred the electrical data from the electrodes in the ground to the SuperSting computer data collector utilized for this work. The white cylinder below the sprinkler tripod is the rain gauge used for measuring precipitation. 28 electrodes at 0.4 meters spacing were utilized for the experiment..... 8

Figure 2 - Setup for field TERI experiments. A) Location of processed data nodes after inversion of TERI datasets relative to the location of the artificial macropore and the electrodes for a 0.4 meter spacing experiment. B) Field photo of Stillwater, OK field site with metal rod used to generate artificial macropore and simulate saline fluid in macropore. C) Schematic Diagram of artificial macropores in field setting relative to entire TERI domain and 28 electrode setup..... 9

Figure 3 - TERI results from the Oklahoma field experiment with two different wetting sources at 0.4 meter electrode spacing. A) Metal rod source location indicated by black line. B) 20 L wetting source located at same lateral location as metal rod source. Note increase in noise from background data over time as data collection occurred after some ground heating occurred relative to the first wetting experiment. 15

Figure 4 - Vertical profiles for single macropore resolution experiments with two different wetting sources. A) Single metal rod simulating a saline macropore with no lateral flow away from the macropore. B) Twenty liters of water added to macropore to generate a wetted zone around the macropore to increase the conductance of the area. 17

Figure 5 - Lateral effects showing all wetting sources for the single artificial macropore experiment at a TERI image horizontal profile. Gray line represents the metal rod signal, the orange line is the 2 liters of water signal and the blue line is the signal generated by 20 liters of water. The location of the artificial macropore laterally is indicated by the vertical gray line. The location of the electrodes for the 0.4 meter spacing relative to the datapoints is provided as blue crosses..... 18

Figure 6 - Lateral changes in bulk electrical conductivity in a three artificial macropore experiment (macropore locations as vertical lines) that had artificial precipitation applied first to produce an unsaturated upper boundary condition (orange line). The center macropore was then saturated using a macropore infiltrometer during the next TERI experiment (blue line). ... 19

Figure 7 - Vertical profiles of TERI datasets at the location of artificial macropores for coarse (C) and fine sites (F). Unsaturated wetting conditions were generated with a sprinkler. A continuous flow from a macropore infiltrometer was used to generate a saturated profile. 19

Figure 8 - Diagram depicting the wetting domain in the NC site where wetting front velocity analyses were made. Line 1 is parallel with flow while line 3 is perpendicular to flow crossing line 1 and the wetting domain. These lines are the principal investigation of this chapter. Lines 2 and 4 are greyed out due to insignificance in the study. 28

Figure 9 - Field photo of the entire wetting domain in the North Carolina site. Line 1 is on the left, line 2 is on the right. The wetting source is the black and white pvc pipe in the foreground, Soil pits are covered in blue tarps 29

Figure 10 - Field photo of the wetting source for the wetting domain in North Carolina. 31

Figure 11 - A) Electrical resistivity profile for line 1 longitudinal to the flow of the runoff flume. B) Electrical resistivity profile for line 3 transverse to the flow of the runoff flume. Orange outlining indicates the sections where unsaturated flow was interpreted as migrating through the soil zone. Soil hydraulic conductivity was calculated in tables 2 and 3. 35

Figure 12 - A) Change in Electrical conductivity profile of line 1. B) Change in electrical conductivity profile of line 3. Orange outlining indicates the sections where soil hydraulic conductivity was calculated in tables 2 and 3 indicating the zone where fluids migrated through the vadose zone during the experiment. 36

Figure 13 - Interpreted soil matrix flow observed 3.5 m laterally along Line 1. This is indicated through peak values on each curve moving down with moderate changes in conductivity. Green dots indicate peak resistivity values used for wetting front hydraulic conductivity calculation ... 38

Figure 14 - Interpreted macropore flow observed 7.5 m laterally along line 1. Interpretation of macropore flow supported by depth of peak value reached with second curve (2.5 hrs) and staying consistent for each subsequent curve, as well as greater magnitude change in conductivity above 100% during the wetting period 38

Figure 15 - Interpreted lateral flow observed 3.5 m along transverse line 3 outside of the reaches from the wetting source. This location is 1.2 m away from the edge of the surface wetting domain. In this pattern, changes are smaller at the surface and larger at the bedrock boundary. 39

Figure 16 - No flow interpretation observed 8.5 m along transverse Line 3. This location is 2.4 m away from the edge of the wetting domain where no moisture is expected to have changed during the experiment. The largest change in this pattern of the domain is a small negative

change 18 hours after wetting was discontinued which could be attributed to the surface soil drying during the day. 39

CHAPTER I

INTRODUCTION

Modern agricultural practices include the use of fertilizers and pesticides that may be transported from fields to adjacent streams during precipitation events, resulting in impacts to surface water. Riparian buffers are vegetation strips that offer streams and other surface water reservoirs protection from the contaminant runoff (Edwards et al., 1988. Larger buffer zones are not always an ideal solution for limiting runoff because larger zones create a land productivity issue (Weiler and Naef, 2003a; Lee et al., 2004). Thus, it's vital to determine size and location to place the buffer zone to satisfy both runoff prevention and optimal land productivity. The majority of runoff may enter surface water via preferential flow paths. Knowing the hydrogeological properties and distribution of features such as macropores will increase the efficacy in determining buffer zone dimensions. (Weiler and Naef, 2003b).

In order to improve macropore characterization in riparian areas, this thesis evaluates the use of temporal electrical resistivity imaging (TERI) to detect macropores or areas with macropores affecting subsurface flow. The first objective for this project is to determine if macropores can be detected with TERI. We present the field design of macropore detection experiments followed by the design of the ERI setup. A number of methods were used to simulate adding fluids to macropores with these wetting approaches detailed. The set of TERI experiments to evaluate macropore detection are presented in Chapter 2.

The second objective for this project is to detect macropores using TERI through tracer velocity analysis of TERI data. Tracer velocity is the speed at which added water moves through a section of the test plot vertically. Vertical profiles along the ERI lines are used to calculate wetting front velocities that can be combined over a number of different temporal datasets to create a hydraulic conductivity map of the subsurface in the TERI domain. This set of TERI experiments are presented in Chapter 3.

CHAPTER II

DETECTING MACROPORE FINGERING USING TEMPORAL ERI

INTRODUCTION

Modern agricultural practices use fertilizers and pesticides that may be transported from fields to adjacent streams during precipitation events, resulting in negative impacts to surface water. Riparian buffers are vegetation strips that offer streams and other surface water reservoirs protection from the contaminant runoff (Edwards et al., 1988). Simply creating larger buffers zones is not ideal for stopping the most runoff because it creates a land productivity issue (Weiler and Naef, 2003a; Lee et al., 2004). Thus, it's vital to determine size and location to place the buffer zone to satisfy both runoff prevention and optimal land productivity. Knowing the hydrogeological properties of geological features such as macropores and gravel outcrops would increase the efficacy in determining buffer zone dimensions. (Weiler and Naef, 2003b).

The current design of conservation practices such as vegetative filter strips and riparian buffers focuses solely on surface runoff with subsurface nutrient transport assumed to be negligible (Fox, 2019). However, subsurface transport can become significant with preferential leaching and can negate the intended benefits of these widely adopted control practices (Fuchs et al., 2009). In fact, when observing the functioning of riparian buffers, practitioners commonly find that the observed hydrologic response of the system suggests a much higher infiltration capacity than expected based on soil texture or matrix infiltration experiments alone (Sabbagh et al., 2009, Heeren et al.,

2015). To limit degradation of ecosystem services and improve land use efficiency, research is needed on understanding and incorporating the influence of preferential flow in buffer design (Orozco-Lopez et al., 2018; Fox, 2019).

It is difficult to classify a macropore based on a predetermined size because of soil heterogeneity. For this reason, the definition of a macropore is a pore that exhibits preferential channeling of fluids in comparison to other pores in the surrounding strata (Beven and Germann, 1982). This preferential channeling has made computer modeling of macropore flow historically problematic. According to Skovdal Christiansen et al. (2004) and Jarvis et al. (1991) the largest uncertainty with modeling macropore flow remains the behavioral changes between saturated and unsaturated upper-boundary conditions. Apart from saturation, soil type and heterogeneity are major compound factors for preferential flow in macropores. This was indicated in the studies on tillage in fields which have shown the concentrations of dissolved phosphorus in precipitation event water was much greater in no-till fields (Williams et al., 2016). Disturbing the soil can help reduce the risk of phosphorus transport from tile-drained fields. In places that cannot be tilled, especially near any adjacent stream to a field, mapping the area for preferential flow paths can aid runoff prevention efforts using accurate buffer zones.

Soil texture and soil moisture content both impact the occurrence and prevalence of preferential flow in soils (Simunek et al., 2003; Orozco-Lopez et al., 2018). Preferential flow has been observed to occur in a variety of soil textures. For example, a meta-analysis performed by Koestel et al. (2012) on the impact of macropore flow on solute breakthrough curves suggested that moderate macropore flow was only possible above a threshold of 8% clay content. Also, macropore flow has been observed to generate at near saturation, proposed by some authors to be 6 to 10 cm when the water pressure exceeds the required entry pressure of the pore interface (Jarvis and Larsson, 2001; Jarvis, 2007). Furthermore, the interaction of this macropore flow with the presence of a shallow water table may also be of more importance for riparian buffers

(Orozco-Lopez et al., 2018). The presence of a shallow water table can modify soil water contents in the vadose zone providing greater opportunities for the activation of macropore flow and reduces mass transfer between the matrix and macropore domains. While recent research has suggested that preferential flow pathways can be activated under unsaturated soil moisture conditions, additional research to verify the occurrence of preferential flow under various soil hydraulic conditions such as the presence of macropores or capillary barriers and an understanding of how to detect preferential flow once it activates is critical.

Temporal electrical resistivity imaging (TERI) is a geophysical surveying technique used for evaluating the subsurface. Resistivity measurements have been used since the 1800s to evaluate electrical changes in the subsurface (Van Nostrand and Cook, 1966). Advances in instrumentation and computing allowed temporal resistivity data to be acquired and processed to observe soil fluid movement and lateral migration (Griffiths and Turnbull, 1985; Halihan et al., 2019). While resistivity measurements have existed for a long time, TERI was limited in soil studies prior to sufficient instrumental and computational developments (Yunmoon Jung, 2000; Zhou et al., 2001). As the instrumentation has become more widely available, the differences in resistivity due to the migration of soil moisture have been evaluated for a number of soil properties, most commonly vegetation, water content, and temperature variability (Jayawickreme et al, 2008; Acharya et al., 2017; Dick et al, 2018; Halihan et al., 2019). By being able to define certain soil properties that can change over the time period of the resistivity data set collection, significant insights can be gained into the spatial location and temporal period of soil moisture migration and macropore activation.

One objective of macropore studies is to determine the distribution of macropores in the subsurface and to improve the understanding of their function and how to manage areas with significant macropore flow. Using TERI may allow macropore structure to be delineated by observing where preferential flowpaths occur as the electrical properties change more quickly in

areas affected by macropores (Moysey and Liu, 2012; Menichino et al., 2014). The objective of this research is to evaluate in controlled conditions whether TERI can demonstrate the presence of artificial macropores whose location and dimensions are known a priori. Using a fine grained and coarse grained site, TERI will be used to determine if artificial precipitation or artificial infiltration in a single macropore can be detected. The signal generated from the wetting may either be too weak to be detected compared to background noise or may be too similar to signals generated by soil heterogeneity.

SITE DESCRIPTION

For thorough examination of preferential flow in differing upper-boundary conditions, the experiments were conducted on two field sites. The first site was in Stillwater, Oklahoma, USA (36º06'04.25"N, 97º08'11.01"W). Stillwater has ~89 cm (35 in) of precipitation annually with average high temperatures of 34ºC (94ºF) during the summer and mild to cool winters where temperatures regularly drop below freezing (Zhang and Nearing, 2005; Mullens et al., 2013). The soil surface in the region is characterized by a Grainola-Lucien complex soil and the Permian Garber-Wellington formation lies beneath (Cobb and Hawker, 1918; Lim and Miller, 2004). Grainola-Lucien complex soils are defined by their clay-like appearance and texture. The fine-grained nature of the soil yields limited lateral flow which should indicate higher preferential flow in macropores. Within the survey area, the ground was relatively flat with 24 cm (9 in) total relief and covered with bermuda and fescue grasses, commonly seen throughout Oklahoma. Rooting depth was measured on site, ranging from 8-10 cm. (Figure 1a).

The second field site was in Raleigh, North Carolina, USA (35º45'36.36"N, 78º40;44.79"W). Raleigh has a similar humid-subtropical climate to Stillwater, differing with more annual precipitation of 117 cm (46 in) (Boyles and Raman, 2003). This site contrasts with the site in

Stillwater exhibiting a Pacolet sandy loam at the surface and Late Proterozoic-Cambrian lineated felsic mica gneiss beneath (Cawthorn, 1970). The coarser grain size demonstrated a presence of macropores and higher slope for the site allowed for more preferential pathways and lateral flow than the Oklahoma fine-grained soil. The survey area consisted of bare soil to lightly vegetated woodland on the periphery (Figure 1b). Vegetation in the area included Loblolly pine, red maple, oak genus, butterfly bushes and holly. The plot was adjacent to Walnut Creek, a small-first order stream. According to the USGS 0208734795 streamflow station at South Wilmington St. (1.6 km (1 mile) from North Carolina field site), the discharge for Walnut Creek averaged 38 m3 (1340 ft3) per second in 2019. The average width of the stream is 5.9 m (19 ft).

For the set of experiments conducted to evaluate macropores with TERI, the majority of work was conducted in the Oklahoma site. The site allowed better control of soil moisture changes by providing a slower moving moisture front with well constrained grassy vegetation. The North Carolina site provided a reasonable comparison as the experiments only used artificial precipitation and macropores. This eliminated the variability that would be generated due to macropore structure, precipitation patterns, and riparian vegetation effects. The only requirement of the experimental sites was to provide a different soil hydraulic conductivity. A site with extremely electrically resistive soil (quartz sand with no fines) may impact the results if data quality decreased due to poor electrical coupling. Additionally, a site with significant quantities of roots or hardpan would make it difficult to insert artificial macropores.

Figure 1 - Field sites for TERI experiments. A) ERI line in fine grain soil site in Oklahoma. Orange cable connects 28 stainless steel electrodes at a 1.6 meter spacing in fine soil. B) ERI line in coarse grain soil site in North Carolina. The orange cable connected the electrodes in the ground to the resistivity instrument utilized for this work. The white cylinder below the sprinkler tripod is the rain gauge used for measuring precipitation. 28 electrodes at 0.4 meters spacing were utilized for the experiment.

METHODOLOGY

The design of the field experiments involved determining a set of soil and macropore parameters and scale for the experiment to provide a clear understanding of macropores using TERI. We present the field design followed by the design of the ERI setup. Three methods were used to generate electrical changes due to adding fluids to macropores and these wetting approaches are detailed. Finally, the set of TERI experiments are presented followed by the methods used to analyze the results.

Experimental Field Design:

To determine if TERI would detect a macropore via electrically conductive fingering patterns, a series of field tests were conducted to compare ERI resolution, fluid boundary conditions, and macropore dimensions. An electrically conductive finger pattern should appear as a stripe or streak of increasing bulk electrical conductivity on a TERI dataset. These increases in bulk electrical conductivity in the TERI data are the primary focus to indicate fluid f pathways

provided by macropores. Different wetting approaches separately test saturated and unsaturated upper-boundary conditions. A macropore infiltrometer gradually drained water directly into an artificial macropore and emulated saturated conditions. The same area dried for a couple of hours and was wetted again with a sprinkler simulating rainfall over a larger area, which maintained unsaturated upper-boundary conditions. The artificial macropores were also limited in number and distributed evenly across the line. This was to avoid signal blending from multiple macropores during data processing.

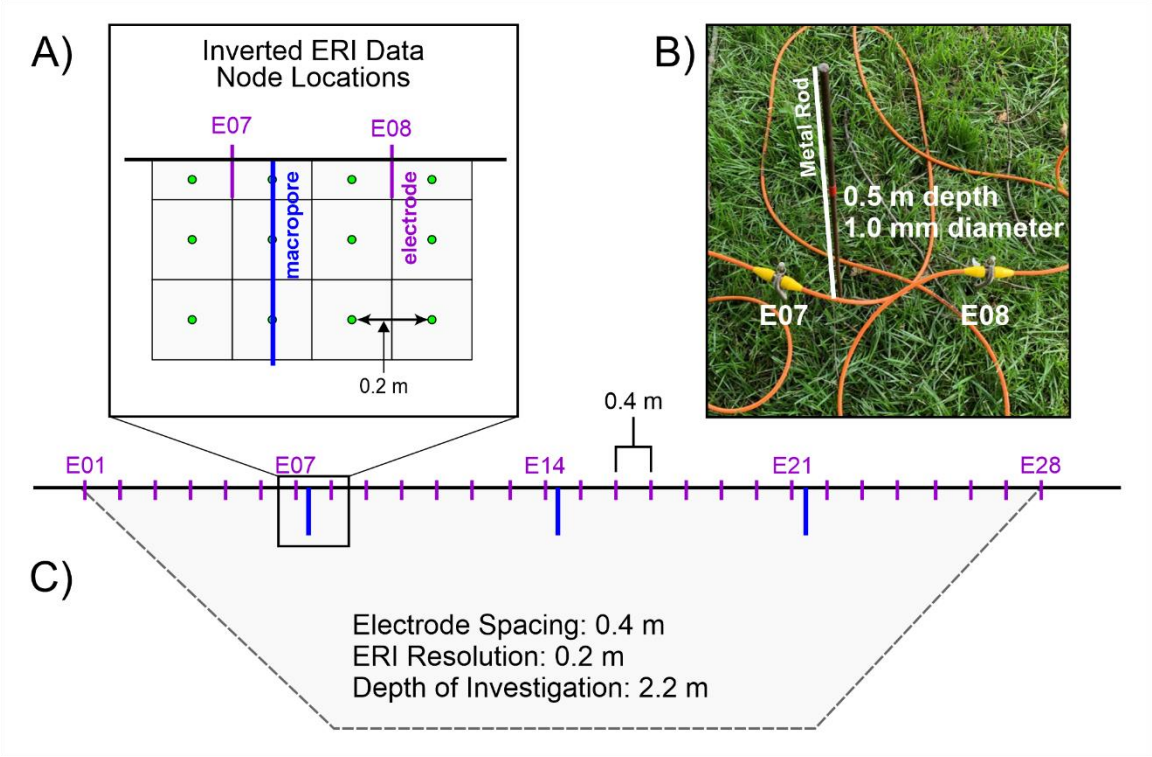

Figure 2 - Setup for field TERI experiments. A) Location of processed data nodes after inversion of TERI datasets relative to the location of the artificial macropore and the electrodes for a 0.4 meter spacing experiment. B) Field photo of Stillwater, OK field site with metal rod used to generate artificial macropore and simulate saline fluid in macropore. C) Schematic Diagram of artificial macropores in field setting relative to entire TERI domain and 28 electrode setup.

ERI Design:

A series of ERI resolution tests were conducted to determine the electrode spacing for maximum temporal dataset quality. ERI experiments rely on a point source approximation for the location of electrodes. Signal is relayed from one electrode to neighboring electrodes for generating a

current field. Thus, getting them too close violates the basic point source assumptions for ERI data collection and limits electrode spacing in the field to about 0.25 meters on practical basis (Van Nostrand and Cook, 1966). On the other end of the spacing scale, too large of spacings would compromise the ability to detect macropore signatures and the signal strength would decrease with increasing image block size (Figure 2). In the first experiment, three overlapping ERI lines with electrode spacings doubling for subsequent experiments were set up along a flat grassy area in the Oklahoma field site. Testing sizes ranged from 0.4 m, 0.8 m, and 1.6 m spacings. Artificial macropores were placed in the middle of each line spacing. The macropores were located at; 5.3m, 11.0m, and 20.4m. Following data collection, the field apparent resistivity data are inverted to generate a modeled resistivity profile (Loke et al, 2003). Regardless of inversion approach, an ERI dataset becomes a smoothed representation of the subsurface variations in electrical properties.

ERI datasets were collected with an AGI SuperSting R8 Resistivity Instrument. The instrument allows a user to collect and store full apparent resistivity datasets. Multiple datasets can be processed to evaluate the changes in bulk resistivity that occurred between datasets to obtain TERI data. A relay switch box and a 28-electrode dumb cable were attached to stainless steel electrodes to survey the field site. To power the instrument for data collection, a gas-powered generator and an AGI power supply box were used to convert the 110 V source from the generator to a 12 V source for the instrument. Once the survey lines were laid out in the field, the SuperSting field computer measured apparent resistivity between electrodes using the Halihan/Fenstemaker method (Halihan et al., 2005; Acharya et al, 2017; Halihan et al., 2019). This robust inversion technique was utilized to convert the apparent resistivity data to modeled electrical resistivity data. These data were differenced in order to obtain datasets of changes in bulk electrical conductivity between datasets (Halihan et al., 2011; Acharya et al, 2017; Halihan et al., 2019).

Wetting Approaches:

In the Oklahoma field site, a metal rod with a diameter of 6 mm was placed in the middle of the ERI line to a depth of 50 cm (Figure 1). The metal rod was left in situ during imaging to simulate a high salinity fluid filling a single macropore. The importance of using this technique lies with the metal rod in a fixed position in the ground having no lateral effects versus wetting the ground with water. The same metal rod was used to generate additional artificial macropores.

Once the artificial macropores were created, the intention was only wet the zone influenced by the artificial macropores. A 5-gallon bucket was utilized to make a macropore infiltrometer. A hole the diameter of the rod was put in the bottom of the bucket; by holding the bucket down over the macropore location, water could be added directly to the macropore. A full infiltrometer would take approximately 30 minutes to an hour to drain into the macropore. This setup allowed partial wetting of the macropore domain with a limited volume of water. In these experiments, we used 2 liters or 20 liters of water to fill the infiltrometer. The setup also allowed imaging of the macropore under fully saturated conditions by continually adding water during an imaging period. The flow rate from the infiltrometer was measured by monitoring the change in water level over time in the bucket and using the hole size for the flow area.

The final wetting method used a sprinkler to wet the survey area while avoiding any pooling of water at the surface. A rain gauge was used to determine the precipitation flux generated by the sprinkler system. The sprinkler was applied to attempt to simulate a large precipitation event over an approximately one-hour period. The method may result in some uneven application of water due to the spray pattern of the sprinklers, but this did not result in visually significant differences in the wetted area. To monitor the soil moisture during the North Carolina experiments, EC-5 soil moisture sensors (METER Environment, Pullman, WA) were inserted at depths of 10, 20, 30 and 40 cm in covered trenches. EC-5 sensors have a measurement volume of approximately 0.2 L and therefore provide near point-scale estimates of water content. The sensors were connected to EM-

50 data loggers (METER Environment, Pullman, WA), recording soil water contents at 1-minute intervals. These sensors confirmed that soil moisture remained below saturation throughout the sprinkler infiltration tests.

Imaging Experiments:

Data collection consisted of three experiments, with sets of imaging sequences where the ERI geophysical surveying was employed. The first imaging sequence involved determining the optimal ERI resolution for detecting a single macropore in the fine soil Oklahoma field site. The second imaging sequence was at the same field site with three macropores across the same ERI line in fine soil. The last and final imaging sequence was in the North Carolina field site, characterized by coarse soil.

For the Oklahoma field site, three electrode spacings of: 0.4 m, 0.8 m, and 1.6 m were alternated between three electrical signal changes, totaling nine TERI datasets for the first sequence. Each signal detection was imaged once for each electrode spacing change. The first set of ERI datasets collected were three background datasets with no macropores, one for each electrode spacing. The first signal detection test was the metal rod left in place at the middle of the ERI line, while spacings were doubled for each of the three images. For the second test, the metal rod was removed from the ground, leaving an open macropore. In place of the metal rod, the macropore infiltrometer was placed and held over the macropore location. Two liters of water was added to the macropore infiltrometer and allowed to fully drain into the macropore for the starting image set with the two-liter source. Finally, the last test in this imaging sequence was fundamentally identical with the second test, utilizing the macropore infiltrometer once more. This time, 20 liters of water was added to the bucket, followed by the final three resistivity datasets being collected. There was an assumption that the wetted domain from a fluid addition would not migrate significantly during the time required to move cables and collect the three datasets at the varying resolutions.

Field Site	Test	Soil Type	Upper-boundary conditions	Electrode spacing (m)	Wetting approach
Fine Soil (OK)	1 macropore	Fine	unsaturated	0.4 0.8 1.6	metal rod
				1.6 0.8 0.4	2 L water
				0.4 0.8 1.6	20 L water
	3 macropores	Fine	unsaturated saturated	0.4	sprinkler macropore infiltrometer
Coarse Soil (NC)	1 macropore	Coarse	unsaturated saturated	0.4	sprinkler macropore infiltrometer

Table 1 - Imaging sequence for the TERI experiments in Oklahoma and North Carolina.

TERI Analysis:

Once each ERI dataset was acquired from the field, they were inverted and differenced to determine the changes in bulk conductance over time (Halihan et al., 2019). The RMS error was evaluated for each ERI inversion and each TERI differenced dataset. The noise levels for the datasets were compared by evaluating two ERI datasets prior to any wetting experiments to determine experimental repeatability of no water being added to the system. Once the noise levels were determined, the data could be evaluated as either an entire TERI dataset that was contoured by value as a 2D dataset or plotted along a line through the data as a 1D horizontal or vertical dataset. To compare different wetting methods, a single vertical or horizontal line of data were extracted from the TERI datasets to evaluate vertical or horizontal changes at the macropore locations.

The analysis to determine the effects of a single macropore first evaluated the effect of TERI resolution. The results of the various spacings were compared for the location of the metal rod. The effects of the various wetting methods were compared for the peak change in bulk

conductance, how well the location and depth of the macropore was detected, and how much lateral signal was available from the various wetting sources. The second analysis involved three macropores evenly spaced over the ERI line to differentiate saturated versus unsaturated conditions. The unsaturated macropores affected by artificial precipitation were compared to the macropore that had saturated conditions throughout the experiment due to the macropore infiltrometer wetting a macropore during an entire imaging event. The final analysis compared the unsaturated and saturated macropores in the fine-grained Oklahoma site against the coarse-grained North Carolina site. The datasets were evaluated vertically at the location of the artificial macropore as well as comparing lateral extent.

RESULTS

The results present the overall data quality of the experiments, which had a low background noise in order to detect some of the effects. First the single macropore experiment with a range of TERI resolution and wetting sources is presented. Second, the multiple macropore experiment results are evaluated and then the third experiment comparing between the coarse and fine-grained sites.

Data Quality:

At the Oklahoma site, there were 15 ERI datasets and 11 TERI datasets. The ERI inversion RMS errors were approximately 2.5%. This was a low error percentage as RMS can be as high as 20-25% and still be considered acceptable ERI data (Zarroca et al., 2015). The TERI differencing datasets had lower RMS differencing error values of approximately 1%. The changes in the difference data increased in the dataset over time in the shallow portion of the dataset, as the ground heated up. This increased from less than a half percent change to approximately 2.5% increase in conductance (Figure 3). The background datasets for the TERI experiments indicated

that less than 0.5% change in conductance was present between datasets due to instrumentation and setup.

The coarse-grained North Carolina field site included 3 ERI datasets and 2 TERI datasets. There was a higher error percentage among ERI datasets from North Carolina compared to datasets from Oklahoma, likely due to site conditions as all datasets had lower errors than many published datasets. ERI RMS error percentages were approximately 4.5%. TERI RMS values were approximately 3%. Less heating occurred on the North Carolina site as it was better shaded than the Oklahoma site. The background datasets for the TERI experiments indicated that less than 0.5% change in conductance was present between datasets due to instrumentation and setup.

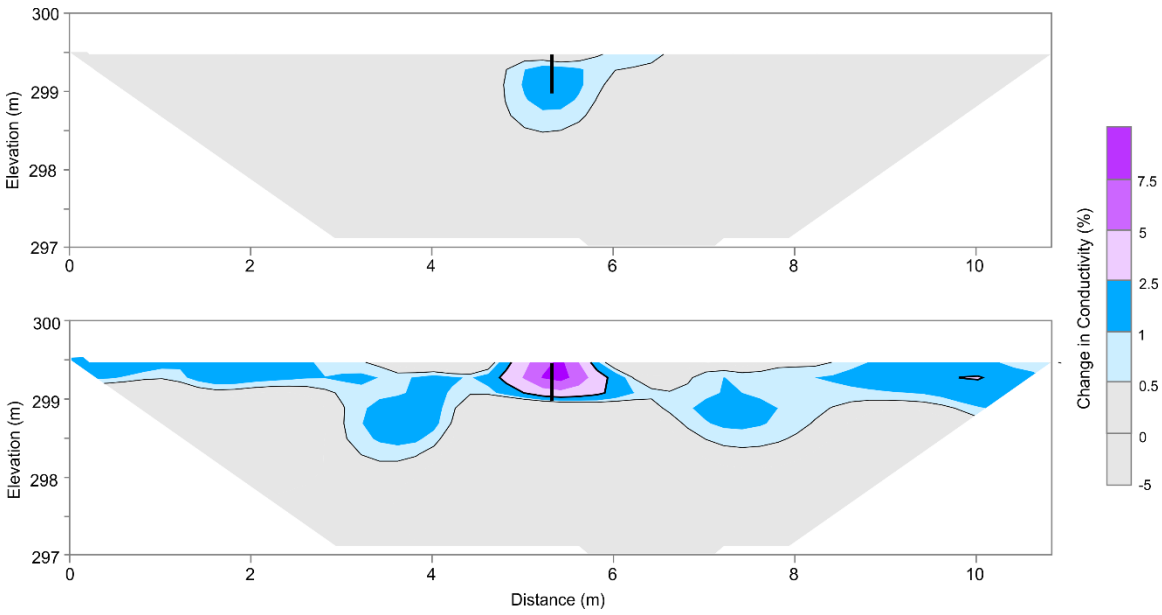

Figure 3 - TERI results from the Oklahoma field experiment with two different wetting sources at 0.4 meter electrode spacing. A) Metal rod source location indicated by black line. B) 20 L wetting source located at same lateral location as metal rod source. Note increase in noise from background data over time as data collection occurred after some ground heating occurred relative to the first wetting experiment.

Single Macropore Detectability:

The effect of resolution from the single artificial macropore experiment provides the data to determine an effective electrode spacing for field investigations of natural macropores. The metal

rod experiment provided a detectable signal of a 1.6% increase in conductance at the location of the rod in the 0.4 meter electrode spacing dataset (Figures 3a and 4a). Data for 1D profiles (Figure 4) come from a single vertical line of data from the larger dataset (Figure 3). This was in a context of noise levels below 0.5% change in positive conductance and below ~1.0% noise levels in negative conductance. In typical field datasets with errors of 3% or higher, the rod would not be detectable in the 0.2 meter block that the technique was evaluating, but in the low noise datasets, it was apparent. At the 0.8 meter spacing, the rod was still detectable above the 0.5% noise level, but at the 1.6 meter spacing the rod was part of the noise. The structure of the data has a negative change in resistivity of less than 1% as part of the signal. The depth of the rod was captured by the dataset as well with the bottom of the rod located adjacent to a peak value detected just above or below the base (Figure 4a). The peak value trends deeper with larger image resolution.

The various wetting sources used for the single macropore experiment allowed larger signals to be generated as a greater volume of the subsurface became wetted. The 2-liter source roughly doubled the signature from the metal rod with a peak conductance change of 2.9%. For the 2-liter source, the 1.6 meter spacing again could not detect the signal from the wetting relative to the noise in the dataset. For the 20-liter source, the signal for the 0.4 and 0.8 meter spacing grew to approximately 9%, and the 1.6 meter spacing generated a change of approximately 3% allowing a detection relative to the noise of the datasets (Figure 4b). The peak values in the wetting sources tended to be at or near the surface with the gradient of the data dropping the value below the noise levels near the elevation of the bottom of the rod. The data also had negative changes in resistivity greater than the noise levels below the detection of the wetted area (Figure 4b). This was interpreted as an effect of the method and not a field change in the bulk conductance of the material.

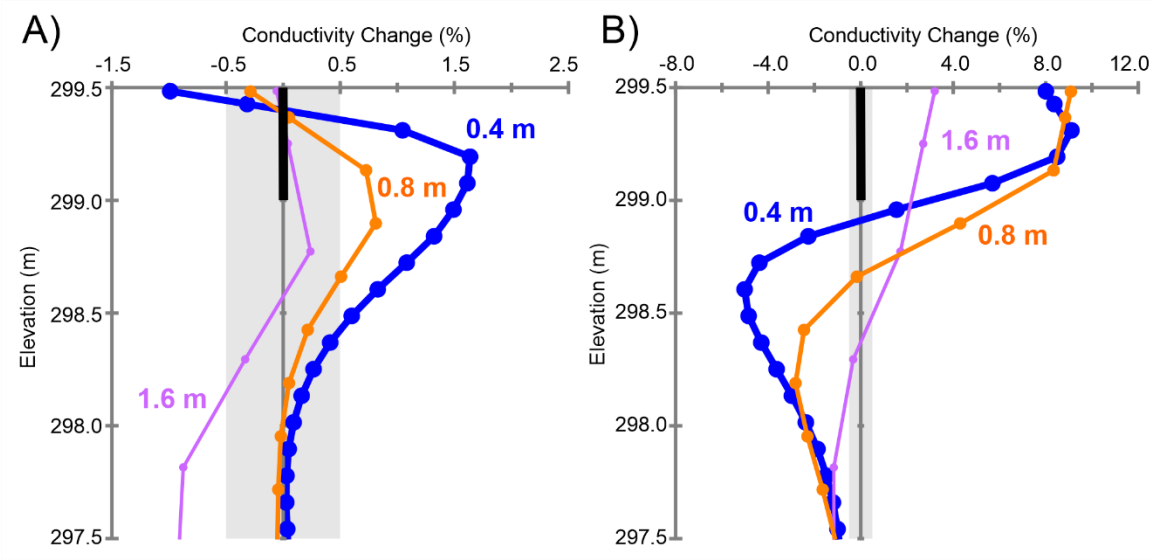

Figure 4 - Vertical profiles for single macropore resolution experiments with two different wetting sources. A) Single metal rod simulating a saline macropore with no lateral flow away from the macropore. B) Twenty liters of water added to macropore to generate a wetted zone around the macropore to increase the conductance of the area.

On a lateral basis, the signals employed in the single artificial macropore experiments should exist in only the region between the electrodes. Only the 20-liter source should have significant potential for higher lateral spread. For all three sources, the location of the macropore was the peak lateral signal (Figure 5). Data from 1D lateral lines (Figure 5) come from single horizon of data in larger dataset (Figure 3). The lateral effects with the presence of the metal rod are displayed as a change in conductance as a distance away from the metal rod's location for the spacings to each side of the rod location. The width of the lateral effects gets larger with increased spacings, but the signal was contained to the data blocks in the adjacent stake spacing location from the location of the artificial macropore (Figure 5). The location was detected properly, with a width of three times the actual location for the macropore.

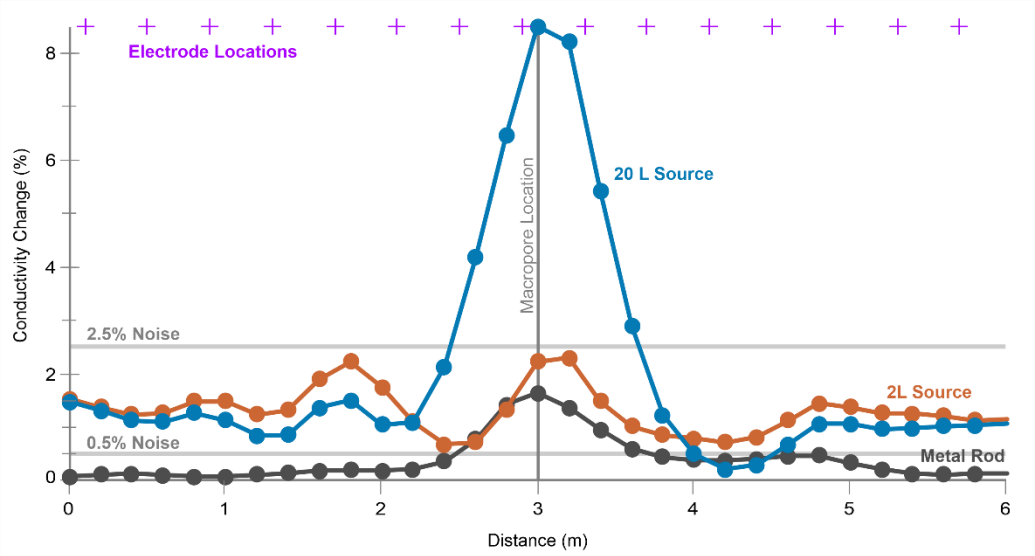

Figure 5 - Lateral effects showing all wetting sources for the single artificial macropore experiment at a TERI image horizontal profile. Gray line represents the metal rod signal, the orange line is the 2 liters of water signal and the blue line is the signal generated by 20 liters of water. The location of the artificial macropore laterally is indicated by the vertical gray line. The location of the electrodes for the 0.4 meter spacing relative to the datapoints is provided as blue crosses.

Multiple Macropores Saturated versus Unsaturated:

The experiment to test multiple macropores allows a comparison between three artificial macropores, two that experience only precipitation and one that experiences a saturated condition after precipitation using the macropore infiltrometer. The results for the experiment on a vertical basis show a similar change with conductivity in relation to depth as the single macropore resolution tests. The peak of conductance changes sharply at the 0.5 meter depth base of the macropores. As expected, the saturated macropore exhibited a larger change conductance than precipitation alone, but not significantly (Figure 6). The bulk conductivity changes between the three macropores was stronger than the single macropore experiment as more water was applied in the experiment. All three macropores appear to have activated during the unsaturated experiment with the sprinkler wetting source.

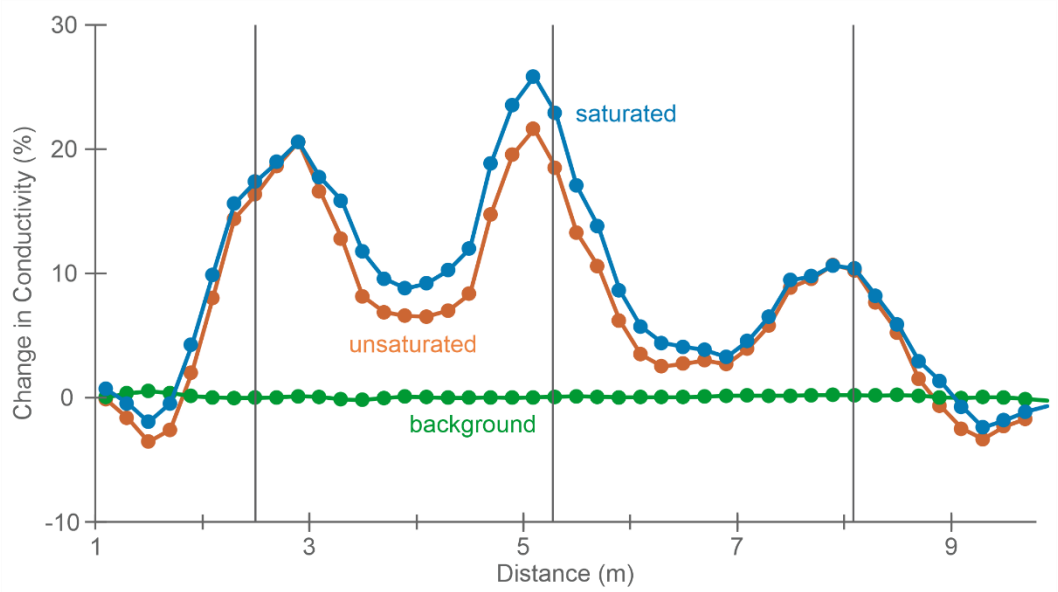

Figure 6 - Lateral changes in bulk electrical conductivity in a three artificial macropore experiment (macropore locations as vertical lines) that had artificial precipitation applied first to produce an unsaturated upper boundary condition (orange line). The center macropore was then saturated using a macropore infiltrometer during the next TERI experiment (blue line).

COARSE SOIL VERSUS FINE SOIL

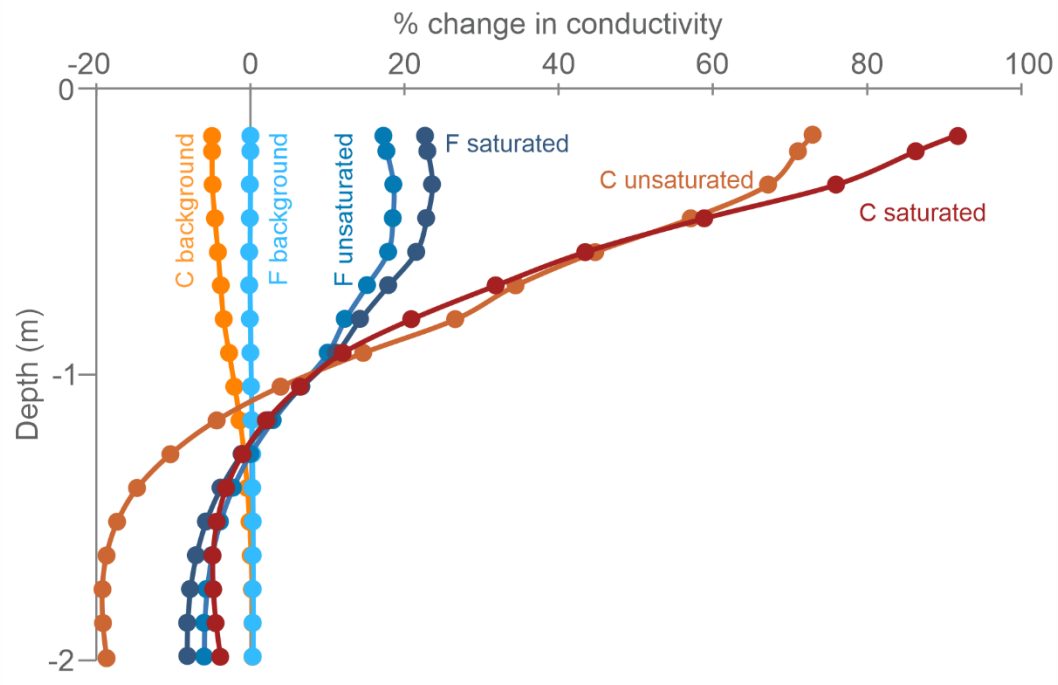

Figure 7 - Vertical profiles of TERI datasets at the location of artificial macropores for coarse (C) and fine sites (F). Unsaturated wetting conditions were generated with a sprinkler. A continuous flow from a macropore infiltrometer was used to generate a saturated profile.

The results for the coarse soil are similar to the fine soil with the unsaturated profiles not qualitatively different in trends relative to the saturated experiments (Figure 7). At both sites, the saturated experiment generated a slightly higher change in bulk conductivity near the top of the profile, but the shape of the resulting signal was otherwise roughly identical. The coarse site had overall larger changes in bulk conductivity based on a different media. No apparent changes in macropore activation were detected between the two sites. Both sites had active macropore flow in both the macropore infiltrometer saturated condition and the high artificial precipitation wetting condition.

DISSCUSSION

The experiments were useful in that by utilizing small time changes in an artificially controlled macropore with artificial precipitation, low noise levels could be achieved that were below normal variations in surficial temperature or soil moisture changes in electrical properties (REF). The experiments allow a measurement of the ER signal generated by a single macropore in the subsurface which is only a signal between 1% and 2% change for a metal rod simulating a macropore filled with high salinity fluids. Under natural field conditions, this signal would be undetectable.

The experiment also allows the data to clearly indicate that negative resistivity changes beneath the wetting signal were not due to soil moisture migration, but simply an artifact of the method. As the experiment had both low noise and low signal, these negative resistivity changes were in some cases similar in magnitude to the wetting positive change in resistivity (Figure 4 and 7). These changes should relate to the location of positive changes in resistivity and should not be interpreted as soil moisture migration, but simply an artifact of the methods used to obtain the numerical profiles.

The questions surrounding macropore detection using TERI are similar among a range of investigators that the experiment was evaluated. First, can the method detect a single macropore, second, how precisely is a macropore located with TERI, and finally, what does TERI indicate about the activation of macropores. These questions are addressed in order below.

Can TERI Detect a Single Macropore?

The metal rod used to simulate a macropore filled with saline fluid with no lateral flow was detectable with high resolution (low stake spacing) and low noise which would not be possible in some soil settings (Mosey and Liu, 2012). The small electrode spacing was repeatable, but difficult to access large riparian areas except at spot locations. The low noise level achieved was not repeatable as other field sites have much higher background noise. Additionally, if the temporal difference between surveys was before and after rain events, the longer time between imaging events would result in greater noise due to heating and vegetative effects (Robinson et al., 2012; Acharya et al., 2017).

Does TERI locate macropores precisely?

In a normal freshwater soil environment, a fluid filled macropore would not provide as great of a resistivity contrast with media as the metal rod did. Detecting an active macropore would require detection of wetted media around the macropore for typical size macropores. The conductive fingering that may be generated may be near a macropore, but lateral migration of fluids will only show the rough location laterally. Additionally, a narrow stronger wetting front would look similar to a broader weaker zone due to the lateral spread of the TERI data. The technique will provide a reasonable estimate for the depth of the macropores if they are responsible for generating the fingering signal. The shape could also be produced by a change in the media other than macropores that is causing a high hydraulic conductivity pathway.

When Do Macropores Activate?

The change in bulk conductivity generated by the artificial macropores wetted by sprinkler was only slightly weaker than the signal obtained by saturation from the macropore infiltrometer. Whether an unsaturated boundary was simulated with a sprinkler, or the macropore infiltrometer provided a fully saturated macropore, there was a higher change in bulk conductivity near the macropores. This indicates preferential flow through macropore activation does not require complete saturation of the upper boundary conditions in these experiments. Artificial precipitation rates were comparable to a heavy rainfall event, so the macropores may not activate under lighter precipitation events. Preferential flow activating under unsaturated flow conditions in riparian buffers suggests macropore infiltration as a significant contributor to total infiltration across a range of storm intensities. Such results further support the need for design tools and analyses that consider preferential flow in quantifying the effectiveness of riparian buffers. Additional research into macropore activation mechanism would be required, but the TERI approach may be useful in evaluating alternative conceptual models.

Future Work

The results suggest TERI can be useful in evaluating macropore flow as a method to detect areas that have changed electrical properties due to changes in soil moisture. However, this detection as a spatial characterization is insufficient to evaluate macropore flow as compared to soil fractures or grain size heterogeneity in the soil matrix. If the subsurface matrix properties are well understood, the TERI data can be used to illustrate where anomalous wetted areas are distributed. The results suggest that mapping macropores with the method may be better achieved by evaluating the rate of changes of electrical properties at a single location as macropore changes should occur more quickly than those due to matrix heterogeneity.

CONCLUSION

Artificial macropores were detected using TERI in a field environment in a fine-grained soil as an increase in bulk conductance finger in the subsurface. In a low noise environment, a 6-millimeter metal rod, simulating a saline fluid filled macropore, was detected using a 0.4 and a 0.8 meter electrode spacing. The detection provided a good depth control and lateral location of the macropore, but a broader lateral extent. When a perimeter around the macropore was wetted with 2 or 20 liters of water, a similar result was obtained with progressively stronger signals.

Experiments in fine and coarse-grained soils at two sites in the USA, Oklahoma and North Carolina demonstrated that artificial macropores can activate under both unsaturated and saturated surface conditions. The unsaturated conditions were generated by sprinklers simulating a large rain event and the saturated conditions were generated by a macropore infiltrometer consisting of a bucket with a macropore size hole used to feed water directly into an artificial macropore. While the magnitude of the change in bulk conductance was different in the different sites, the response measured by the TERI datasets was similar between the two sites.

CHAPTER III

TRACER VELOCITY MAPPING OF ALLUVIAL SOIL USING TEMPORAL ELECTRICAL RESITIVITY IMAGING

INTRODUCTION

Preferential flow in soils can occur along any path of least resistance. The most common preferential pathway in soils are macropores, which are pores that vary in size and allow for rapid fluid migration in comparison to the surrounding strata (Beven and Germann, 1982). Macropores account for only a small percentage of total pore space in soils, yet they can dominate the flow and transport behavior, especially during heavy precipitation events. (Beven and Germann, 1982; Jarvis, 2007). This is important for modern agricultural practices which include the use of fertilizers and pesticides that may be transported from fields to adjacent streams during precipitation events, resulting in impacts to surface water (Moysey and Liu, 2012). Noninvasive tools like electrical resistivity monitoring could provide significant insight into the behavior of macropores in soils at the landscape scale. This research focuses on using temporal electrical resistivity imaging (TERI) to determine if macropore flow and associated increases in soil hydraulic conductivity can be mapped in the subsurface based on a set of TERI profile datasets.

In a recent study by (Shanahan et al., (2015) electrical magnetic induction (EMI) measurements from several field sites surveyed by Butt Close and Warren Field were taken and placed in an Markov chain Monte Carlo (McMC) algorithm which took measurements of electromagnetic induction from 10 cm depth intervals and made a distribution calculation for a normalized histogram per depth interval of the density of predicted soil hydraulic conductivity values per 10 cm depth interval. This histogram generates a representative curve for electrical conductivity in relation to soil moisture with depth. However, the algorithm assumes a uniform soil horizon.

The field site in this investigation does not have a uniform soil composition, which could alter the soil moisture profile. To account for this, previous works by (Minet et al., 2011) used GPR (Ground Penetrating Radar) data based on the propagation of an electromagnetic wave in a multi-layered soil horizon. The GPR datasets were inverted from four configurations fitting a two-layered soil moisture profile. Each configuration was derived from fitting the parameters to a Van Genuchten soil model. The parameters determined the configurations through a best fit calculation. As a result, this study created a reference soil moisture profile using Van Genuchten parameters of GPR data in a multi-layered soil column.

Reference soil moisture profiles were used in previous studies using ERI (Mishra et al., 2015). Soil profiles were modeled from irrigated fields across the United States (Mishra et al., 2015). ERI datasets were combined to create vertical soil moisture profiles based on the principle of maximum entropy (POME). An additional important factor of this study is the curves for the soil

profiles were based on three types of wetting events: long time after rain/irrigation, short time after rain/irrigation, and immediately after rain/irrigation. Soil moisture profiles generated from this method provide a framework for interpreting the vertical data profiles evaluated with TERI analysis in this research. While (Mishra et al., 2015) shows a representative soil moisture curve based on wetting events, a uniform soil column is assumed. Lastly, there are limiting factors using POME which include the total probability constraint and the mass balance constraint.

Other work has been done to directly evaluate the variation of hydraulic conductivity at field sites to assess preferential flow. Sudicky (1986) collected permeability measurements across a series of cores along two cross sections, one along and the other transverse to the flow direction. Along the two cross sections, a regular-spaced grid of hydraulic conductivity data with 0.05 m vertical and 0.1 m horizontal spatial discretization revealed that the aquifer is comprised of numerous thin, discontinuous lenses of contrasting hydraulic conductivities. Sudicky (1986) created a soil hydraulic conductivity table of the Borden Aquifer based on estimations and calculations to input into predictive models of flow and transport.

The primary objective of this research is to evaluate preferential flow via mapping hydraulic conductivity with TERI profiles of alluvial soils. It's hypothesized that TERI will work with mapping hydraulic conductivity because changes in electrical conductivity over time should show fluid migration through pulses of increased electrical conductance generated from soil wetting. This coupled with the amount of time it takes for the pulses to wax and wane in a profile could delineate flow and allow tracer velocities to be quantified. Combining several TERI profiles in proximity will yield a map of the hydraulic conductivity over an area where preferential flow can be determined by localized K values in relation to one another.

SITE DESCRIPTION

The field site was a 2 x 10 m test plot located in Raleigh, North Carolina, USA (Figure 3.1). Raleigh has a humid-subtropical climate, with an annual precipitation of 117 cm (46 in) (Boyles and Raman, 2003). This site is characterized by a Pacolet sandy loam at the surface and Late Proterozoic-Cambrian lineated felsic mica gneiss beneath (Cawthorn, 1970). The survey area was situated over bare soil with vegetated woodland on the periphery. The plot was adjacent to a small, first-order stream which empties into Lake Raleigh. The test area was designed perpendicular to the contour of the soil to provide a downhill surface runoff longitudinal to the plot. Bedrock depth varies but is approximately 0.7 m from surface. Visible macropores are evident on the edge of the plot in the bank of the stream. This aligns with the sharply sloped topography at the end of the wetting domain, leading to the stream (Figure 3.2). Prior to the slope is a flat area varying by a few cm in relief across the plot. The area itself is 87 m above sea level and located 35°45’36.63”N 78°40’44.23”W.

The test plot was bounded on the sides using landscape edging and consisted of four ERI lines, five test pits with soil moisture probes, and a wetting source. Figure 8 below depicts the plot with spatial relationships; including a 0.8 m distance between lines 1 and 2 and 2.0 m distance between lines 3 and 4. The wetting source was a 2 meter wide PVC pipe located 1.5 m down from the start of lines 1 and 2. The soil moisture probes along each side of the wetting domain are part of the experiment conducted by (Guertault, et al, 2019) which were in soil pits covered with blue tarps (figure 3.2). Figure 3.2 shows just the wetting domain, with the view from the beginning with the wetting source in the foreground, looking down toward the end of the ERI lines within

the wetting domain. Note the drop in topography at the end of the image, this is the location of the visible macropores and a steep slope for the stream bank.

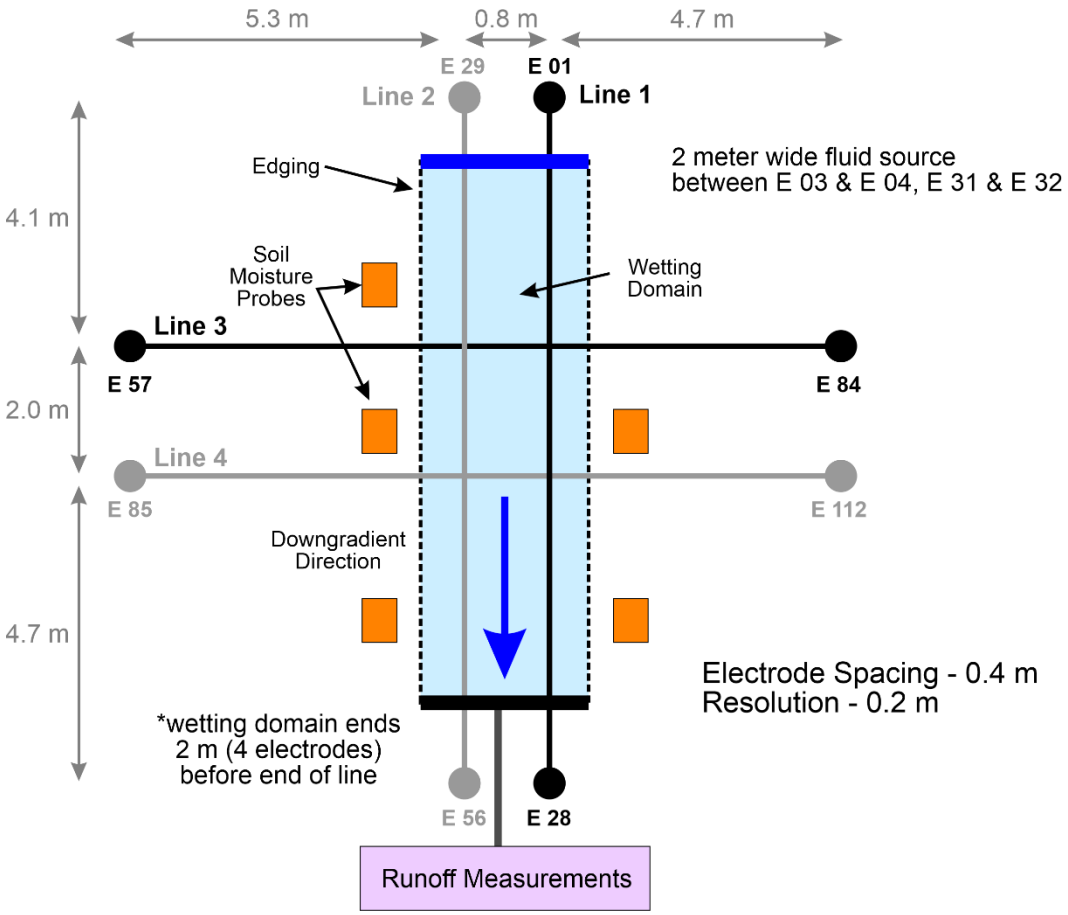

Figure 8 - Diagram depicting the wetting domain in the NC site where wetting front velocity analyses were made. Line 1 is parallel with flow while line 3 is perpendicular to flow crossing line 1 and the wetting domain. These lines are the principal investigation of this chapter. Lines 2 and 4 are greyed out due to insignificance in the study.

Figure 9 - Field photo of the entire wetting domain in the North Carolina site. Line 1 is on the left, line 2 is on the right. The wetting source is the black and white pvc pipe in the foreground, Soil pits are covered in blue tarps.

METHODS

In order to conduct this experiment, a test plot was constructed perpendicular to the elevation contours. The test plot included: a wetting source to saturate the domain perpendicular to the stream, four ERI lines, and a TERI analysis of the data gathered to visualize what happened

during the experiment. The experiment was constrained to the area of the testing plot using landscape edging. Additional experiments were performed using soil test pits Guertault et al., (2019).

The plot included four ERI lines that crossed perpendicularly to each other in pairs (Figure 8). Two of the lines were largely inside the experimental wetting domain and are referred to as the longitudinal lines. The other two lines only crossed through the domain and are referred to as the transverse lines. This wetting domain and specifically one ERI line of each orientation (ERI lines 1 & 3) are the primary focus for this section (Figure 8). Line 1 is parallel with flow and exhibits the most change in topography. Line 3 is perpendicular to flow and crosses the wetting domain as well as line 1. This line is relatively flat with little changes in topography. Lines 2 and 4 collected data but are not included in the analysis, thus they are greyed out. The wetting domain was fenced in on three sides with landscape edging and precipitation measurements were taken through the discharge pipe (Figures 8 and 9).

Wetting Methods:

The objective in this experiment is to attempt to detect macropore flow with saturated upper boundary conditions. In order to saturate the upper layer of the survey area, a 2 meter-wide flume was connected to a standard garden hose and dispersed water evenly over the wetting domain via 1.5 cm diameter holes in a piece of PVC pipe across the flume (Figure 3.3). Discharge measurements from the runoff pipe at the end of the plot domain indicate that the flume equated to 0.17 l/s (2.69 gpm) based on an average of discharge collections in a small 2-liter bucket during 30 second intervals.

Figure 10 - Field photo of the wetting source for the wetting domain in North Carolina.

TERI Data Collection Methods:

ERI datasets were collected with an Advanced Geosciences, Inc. (AGI) SuperSting R8 Resistivity Instrument. The instrument allows a user to collect and store apparent resistivity data. Multiple datasets can be processed to evaluate the changes in bulk resistivity that occurred between datasets to obtain TERI data. A relay switch box and four 28-electrode dumb cable were attached to stainless steel electrodes to survey the field site (Figure 9). To power the instrument for data collection, a gas-powered generator and an AGI power supply box were used to convert the 110 V source from the generator to a 12 V source for the instrument. Once the survey lines were laid out in the field, the SuperSting field instrument measured apparent resistivity between electrodes and the data were processed and differenced using the Halihan/Fenstemaker algorithm (Halihan et al., 2005; Halihan et al., 2019).

Five TERI datasets were collected for the experiment, two during soil wetting and three during drying. There were replicate samples longitudinal to flow and transverse to the flow. The best datasets from each direction were selected for analysis (Figure 8). The first TERI dataset occurred after 30 minutes of wetting and the second at 2.5 hours of wetting. Thereafter, the time elapsed was a drying time since the water source was discontinued. Datasets were collected at 2, 7.5, and 18 hours after the wetting had ceased. Electrode spacing was 0.4 m, yielding a spatial resolution of 0.2 m.

TERI Analysis:

Once each ERI dataset was acquired from the field, they were inverted and differenced to determine the changes in bulk conductance over time (Halihan et al., 2019). The RMS error was evaluated for each ERI inverted model resistivity dataset and each TERI differenced resistivity dataset.

To evaluate vertical wetting along a single 1D pathway, a single vertical line of TERI data was extracted from the datasets to evaluate vertical changes due to water migrating downward in the profile. Wetting curve profiles were created along TERI lines 1 and 3 every meter laterally from the left end starting at 1.5 m and ending at 8.5 m. Hydraulic conductivity values were calculated from the vertical profiles (Figures 13-16) by looking for the peak conductivity change and equating the depth of the peak change with the distance that the wetting front moved vertically into the soil. The vertical distance between peak conductivity change values on each curve against time from the last peak value provides as distance per time interpreted as a soil hydraulic conductivity value.

After evaluating the data and extracting vertical data for each time period, every plot location per meter had vertical velocities calculated based on peak values with time curves. The values are taken from peak points where data values are taken from the equipment with depth against change in electrical conductivity. Every change in peak values from the time curves tells how far the water moved, distance between peak data points, over the time elapsed between each 1D curve. If no changes were detected between datasets, the vertical velocity was determined to be zero. This was common at a depth similar to the known bedrock contact. Results were compounded into a table to better visualize the different velocities calculated laterally along the line.

RESULTS

The first analysis in this section focuses on resistivity data quality which is of significance for temporal data evaluations as errors in a single dataset can be compounded in temporal comparisons. Next, the range and trends of resistivity values are evaluated in the first imaging sequences of the experiment to determine background resistivity changes (Figure 11). Once the background is established, the range and trends of temporal changes can be analyzed with subsequent imaging of the wetted plot compared to the background (Figure 12). After each vertical profile has been processed, the types of temporal changes are evaluated next. The four types of flow observed using TERI data are: macropore flow, lateral flow, matrix flow, and no flow. Using these vertical profiles will ultimately be used to create a map of varying hydraulic conductivities across the plot.

Data Quality:

TERI datasets collected from the NC field site wetting domain were inverted and differenced. Line 1 and line 3 were chosen for analysis due to their low RMS error values. The RMS errors for Line 1 averaged 4-8% RMS and line 3 was 3-6%. To discern between noise and signal, the trends and ranges of resistivity values as well as temporal changes are observed in detail. It's important to keep in mind that for a given soil, the four main controls on the apparent resistivity bounds are the total dissolved solids (TDS) of the fluid filling the macropores and the matrix pores, the saturation of the soil matrix, and the fraction of the soil filled with active macropores (Moysey and Liu, 2012). The data for lines 1 and 3 were then tabulated in Microsoft Excel to show vertical profiles of the ERI lines during and after wetting. The data plots were compared to soil moisture profiles found in previous studies (Mishra et al., 2015).

Range and Trends of Resistivity Values:

Static apparent resistivity images used as backgrounds for temporal analysis provide a range of resistivity values for the subsurface, denoting features such as lithological changes. Readings from 200 – 2000 ohm-m are colored in burgundy interpreted to correspond largely to the soil matrix. These values are relatively high for soil indicating a high porosity soil without significant amounts of electrically conductive clays. Measurements that are greater than 2000 ohm-m is interpreted as low porosity bedrock which is scaled in grey colors (Figure 11). Apparent resistivity of igneous and metamorphic bedrock varies from 1,000-100,000 ohm-m (Gunn et al., 2015). Clays and tills have much a lower apparent resistivity averaging 10-1,000 ohm-m (Gunn et al., 2015). Subsequent imaging of the plot after wetting are compared to the static resistivity values seen in (Figure 11) to give a range and trends of temporal changes.

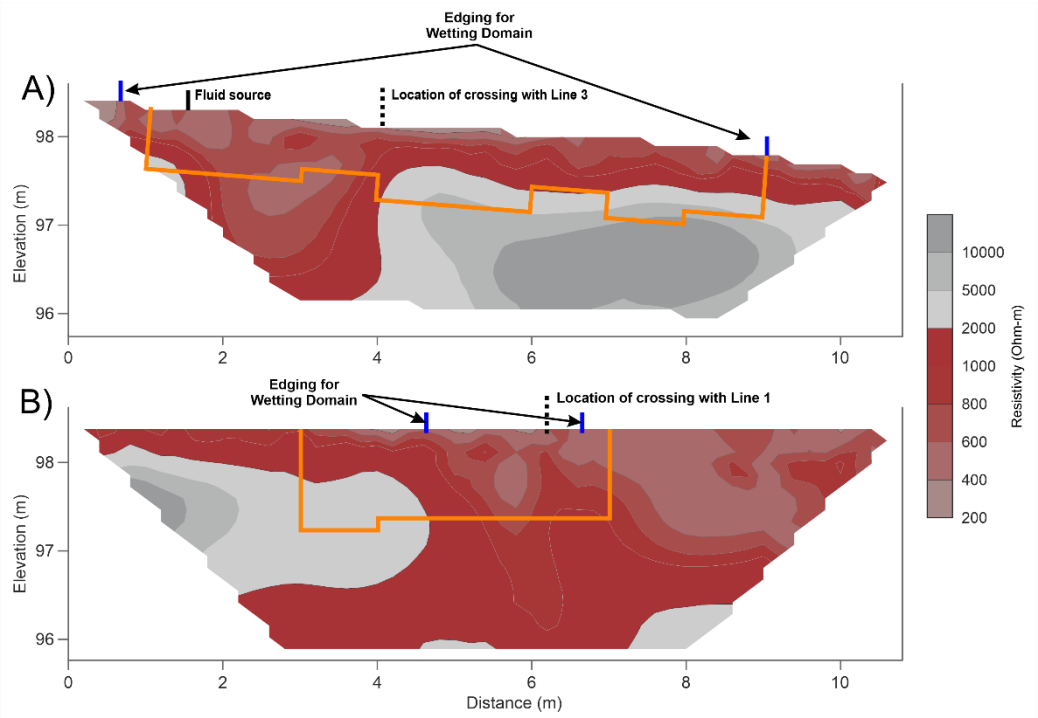

Figure 11 - A) Electrical resistivity profile for line 1 longitudinal to the flow of the runoff flume. B) Electrical resistivity profile for line 3 transverse to the flow of the runoff flume. Orange outlining indicates the sections where unsaturated flow was interpreted as migrating through the soil zone. Soil hydraulic conductivity was calculated in tables 2 and 3.

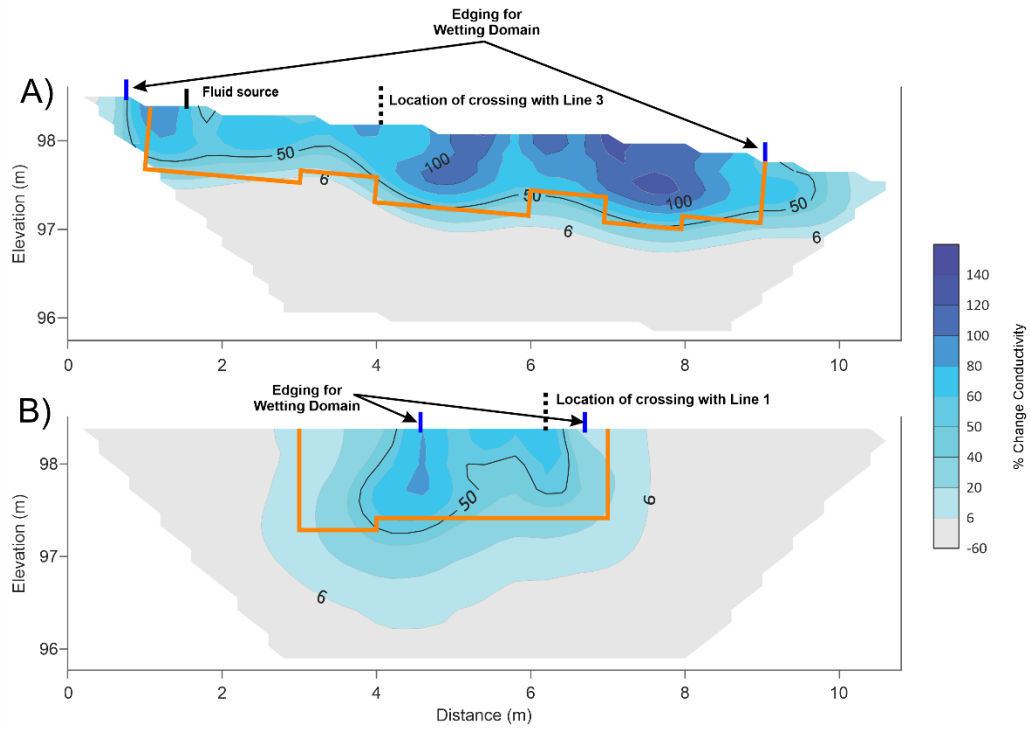

Figure 12 - A) Change in Electrical conductivity profile of line 1. B) Change in electrical conductivity profile of line 3. Orange outlining indicates the sections where soil hydraulic conductivity was calculated in tables 2 and 3 indicating the zone where fluids migrated through the vadose zone during the experiment.

Range and Trends in Temporal Changes:

The change in electrical conductivity over each ERI line that will be examined in detail for wetting front calculation and soil moisture profiles provide the base datasets for the hydraulic conductivity calculations (Figure 12). These TERI images are references for where the wetting front analysis in this experiment are derived. Evaluation of the datasets indicated that background noise levels were approximately 6% (Figure 12) based on evaluating the data where no change should be occurring outside the wetting domain. TERI data above 6% change in electrical conductivity is considered signal indicating locations where soil moisture has changed. Similar changes between 6% and 50% are interpreted as areas dominated by soil matrix flow. Areas that

experienced a change in electrical conductivity greater than 100% are interpreted as likely macropore flow domains as these areas also dried more rapidly. The transition between pure matrix flow and macropore flow areas is between 50% and 100%.

Types of Temporal Changes:

There are four distinct types of patterns distinguished by the wetting curve analysis. Wetting curve profiles were created along lines 1 and 3 every meter from end to end starting at 1.5 m and ending at 8.5 m, respectively. Longitudinal line 1 demonstrates both matrix (Figure 13) and macropore flow (Figure 14) profiles as each flow type is within the wetting domain (Figure 12A). Transverse line 3 includes both lateral flow profiles outside of the flume area (Figure 15) and no flow regions (Figure 16) as this perpendicular ERI line is mainly to characterize results outside of the wetting domain . The resistivity changed the most during wetting with a peak value increasing in depth during the wetting phase. During the soil moisture redistribution phase with no surface water, the change in resistivity decreased over time and progressively deeper in depth for a simple soil wetting pattern which was located near the wetting source (Figure 10).

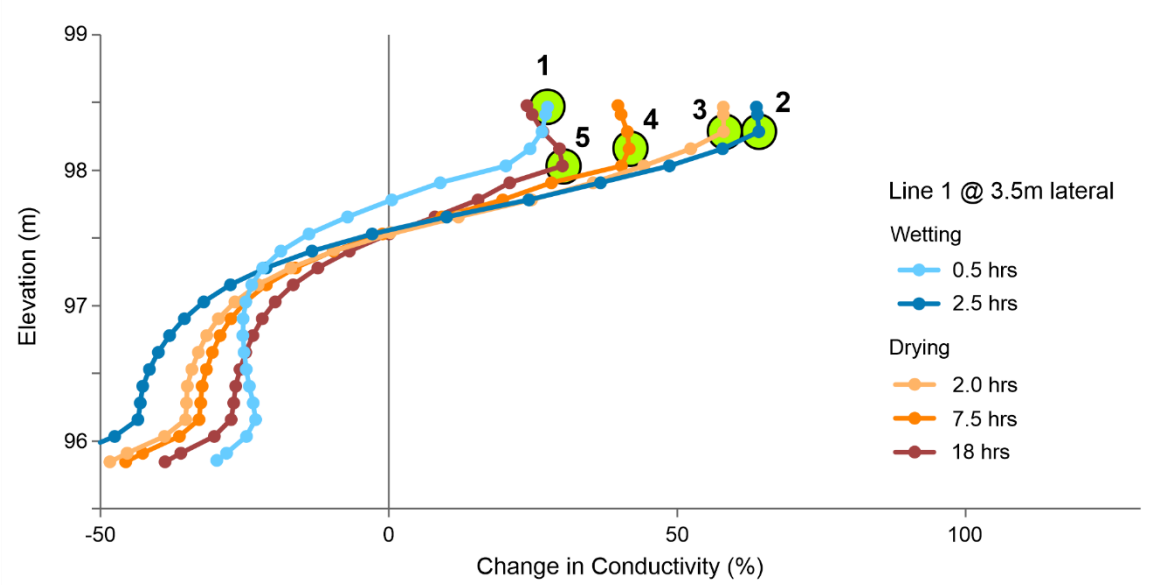

Figure 13 - Interpreted soil matrix flow observed 3.5 m laterally along Line 1. This is indicated through peak values on each curve moving down with moderate changes in conductivity. Green dots indicate peak resistivity values used for wetting front hydraulic conductivity calculation.

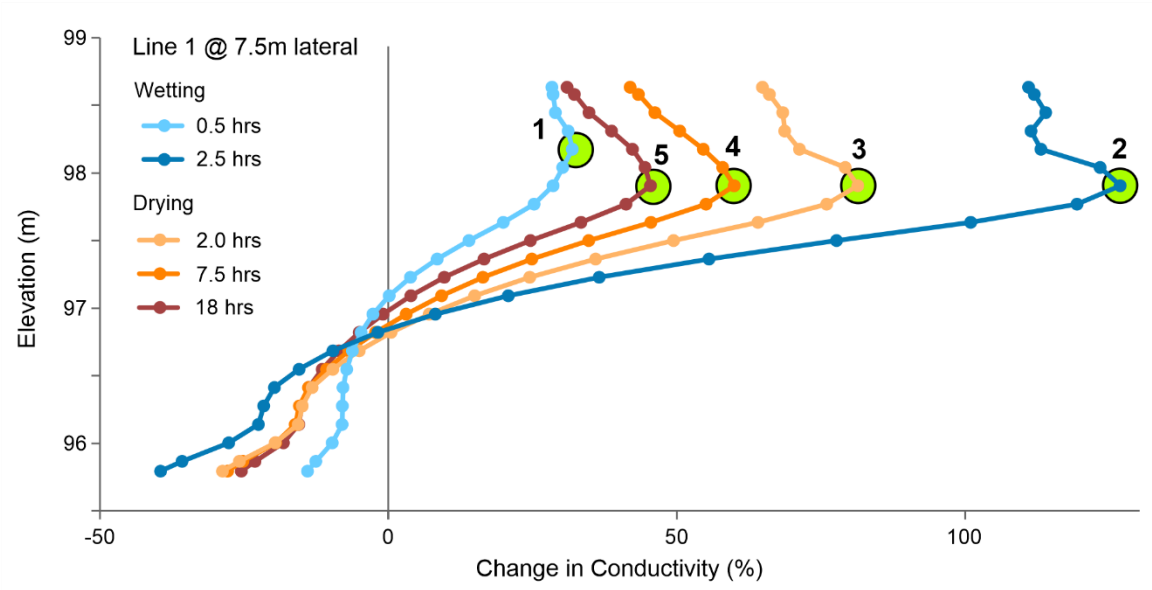

Figure 14 - Interpreted macropore flow observed 7.5 m laterally along line 1. Interpretation of macropore flow supported by depth of peak value reached with second curve (2.5 hrs) and staying consistent for each subsequent curve, as well as greater magnitude change in conductivity above 100% during the wetting period.

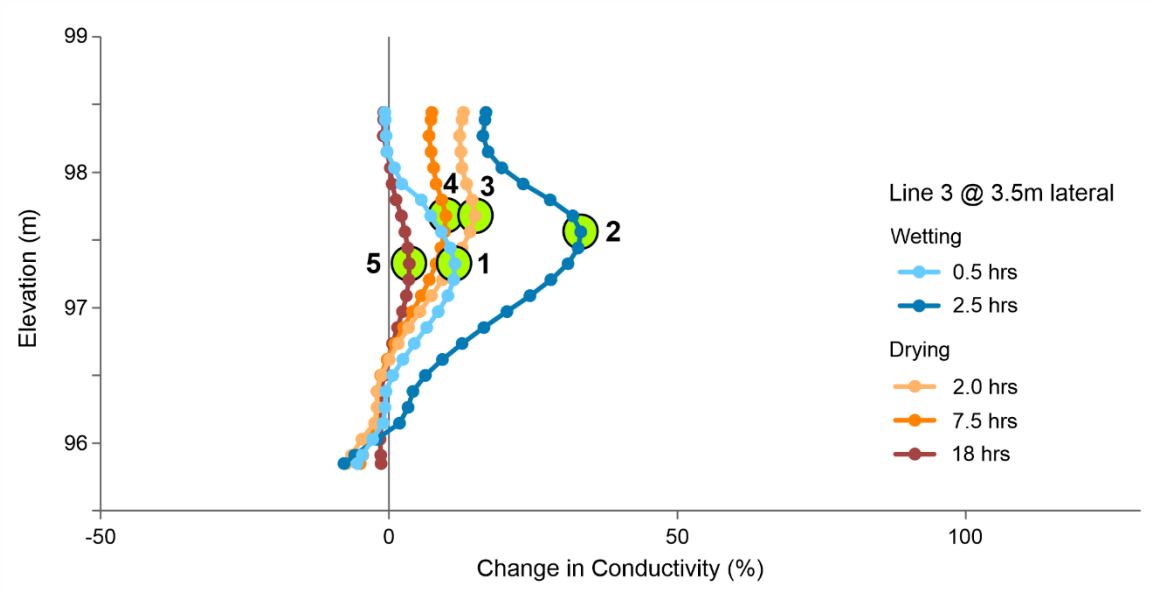

Figure 15 - Interpreted lateral flow observed 3.5 m along transverse line 3 outside of the reaches from the wetting source. This location is 1.2 m away from the edge of the surface wetting domain. In this pattern, changes are smaller at the surface and larger at the bedrock boundary.

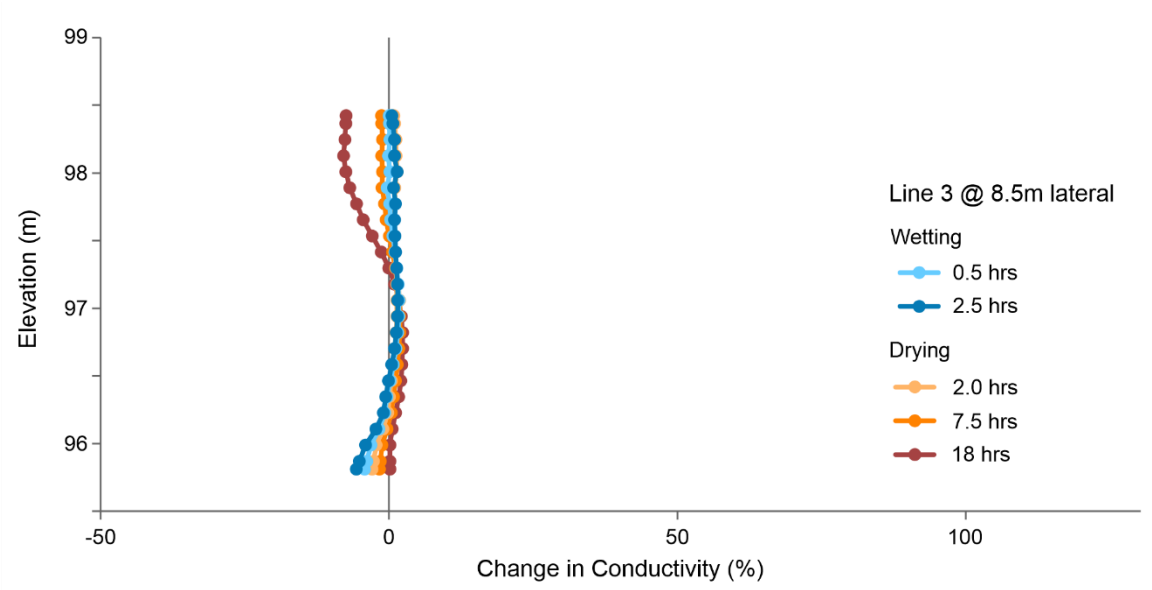

Figure 16 - No flow interpretation observed 8.5 m along transverse Line 3. This location is 2.4 m away from the edge of the wetting domain where no moisture is expected to have changed during the experiment. The largest change in

this pattern of the domain is a small negative change 18 hours after wetting was discontinued which could be attributed to the surface soil drying during the day.

Each flow type has distinctive characteristics that emanate interpretation. Matrix flow (Figure 13) shows a gradual vertical decrease in peak electrical conductivity values, labelled 1 through 5, indicating steady saturation over time. Macropore flow (Figure 14) exhibits a vertical decrease in peak electrical conductivity values from 1 to 2, but 2-5 values plane off with no successive vertical decrease in peak values. This is interpreted as rapid saturation where the wetting front reached a lithological boundary quickly. Matrix flow and macropore flow differ in the time elapsed to reach the same level of vertical saturation in the profiles. Macropore flow is 2-3 orders of magnitude greater in the detected tracer velocity than would occur for matrix flow. Lateral flow (Figure 15) includes changes in electrical conductivity significant enough to record peak values, outside of the wetting domain. The peak values, however, are sporadic and do not follow a pattern similar to matrix and macropore flow. Lastly, no flow (Figure 16) has no peak values as this area was far enough from the wetting domain to remain dry during the entire experiment.

Hydraulic Conductivity Calculation:

The TERI calculated velocities were faster near the surface and slower with depth (Table 2). At approximately ~0.7 m depth, velocities were null due to lack of deeper fluid migration detected in the datasets. This boundary is interpreted as a low permeability bedrock boundary at approximately 0.7 m depth which causes soil water to migrate laterally in the downslope direction that the plume was oriented and corresponds to the soil depth determined from excavation. Calculated velocities change by two orders of magnitude across the plot from 12 to 1740 mm/hr.

The same approach was taken for transverse Line 3 to make a calculated hydraulic conductivity section from compounded vertical profiles. Results yield the same calculated K values for Line 3 at the crossing with Line 1 with a sharp drop to dry vertical profiles at both ends of Line 3 where changes in electrical conductivity did not exceed the background change of 6% increase in conductance.

Depth (m)	1.5	2.5	3.5	4.5	5.5	6.5	7.5	8.5
0.05	360	360	100	1200	960	200	960	360
0.18			65			130		
0.31		65	17					65
0.48	150	17	12			65		36
0.61		12			13		130	
0.74				26				
0.87								

K (mm/h)	Dry/Null	0-50	51-100	101-500	501-1000	1000+

Table 2 - Distribution of calculated tracer velocities based on wetting front velocities in each vertical profile on longitudinal Line 1. The red outlined cell (4.5) represents the location of crossing with transverse Line 3. Results are shown units of in mm/hr. Figure 3.1 shows the location of TERI transects used as data sources for Tables 3.1 and 3.2.

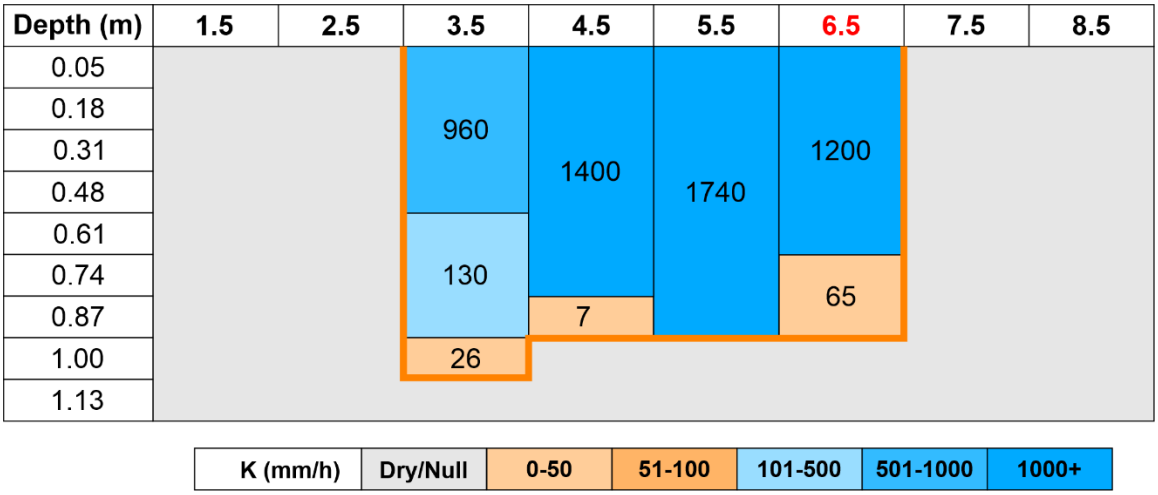

Table 3 - Distribution of calculated tracer velocities based on wetting front velocities in each vertical profile on transverse Line 3. The red outlined cell (6.5) represents the location of crossing with longitudinal Line 1. Results are shown in units of mm/hr.

To calculate the tracer velocities, the peak change in electrical conductivity values from vertical profiles along lines 1 and 3 were taken every meter from 1.5 m to 8.5 m on each line. The peak values are labelled in time order (1-5) (Figures 13-15). Next, the vertical distance measured using TERI data peak grid nodes from the surface was used as the depth of the the wetting front. Each of the five curves on the vertical profiles represent a time that had elapsed in correlation to either wetting or drying of the soil profile. Coupling the vertical distance measured using TERI grid nodes and the time elapsed to for the peak value to get to that position gave tracer velocity as distance over time. Lastly, a unit conversion from m/hr to mm/hr was applied to compare against previous research that calculated soil hydraulic conductivity.

Line 1 shows calculated velocity tracer values between 10-40 mm/hr. These rates are similar for matrix flow from other studies on the same plot (Guertault et al, 2019). Values that are an order of magnitude higher, upwards of 1740 mm/hr indicate macropore flow as these areas wetted and dried much faster than surrounding strata. Lastly, the values for the edge of line 3 would result

from lateral flow as these areas are outside of the wetting domain. This was part of the experimental design to show values for zero change in bulk electrical conductivity or no flow conditions in the soil plot.

DISCUSSION

Can TERI Be Utilized To Calculate Wetting Front Velocities?

The results show wetting curves that are similar in shape to the curves expected for both vertical and lateral migration of fluids in soil over bedrock (Wilson, 2011; Wilson et al., 2018). Around 0.7 m depth, there is a rapid decrease for changes in bulk electrical conductance (Figure 12A) and is similar to the location of the significant change in bulk resistivity (Figure 11A). This depth corresponds to where the competent bedrock limited macropore generation due to further depths but allowed piping processes to develop macropores laterally. The TERI data and subsequent hydraulic conductivity analysis can be compared to what an expected wetting curve should look like along a profile of the line. Once calculated velocities have been established using TERI, they can be compared with velocities obtained using alternative methods to validate the TERI approach. In this experiment, the field plot utilized soil moisture meters in adjacent soil pits Guertault et al. (2021) calculated soil hydraulic parameters by fitting measurements to Van Genutchen parameters. Results from Guertault et al. (2021) in the same field location yield K values between 23-36 mm/hr. Similar values obtained using the TERI approach where results at the base of the soil at 4.5 and 8.5 m share locations with soil moisture probes for the Guertault et al. (2021) experiment (Table 2; Figure 8). The soil moisture probes were located at approximately 0.5 m depth. Locations where the calculated velocities are an order of magnitude higher

interpreted as are where macropore flow is observed. These values may be attributed to a coarse grain matrix, but significant changes were seen in other areas further down the line and near the surface. Macropore flow was also observed out of the profile at the end of the plume confirming the existence of macropores and flow in them during the experiment.

Calculated hydraulic conductivity values in this research have datasets that match the models and data from more traditional sources (Guertault et al., 2021). The change in hydraulic conductivity values within the macropore flow domains are within reason as Mallants et al. (1997) studied macropore flow in three types of soil and found hydraulic conductivity values in coarse-grained soil to have a coefficient of variation (CV) of 619%. This would align with the two orders of magnitude difference between macropore flow and matrix flow hydraulic conductivity values in the results for this research. Finally, a limiting factor for this method stems from the calculated hydraulic conductivity values. Water can move through the survey area too fast for the instrument to image the wetting front location. In some instances, during this experiment, fluid migration reached the interpreted lithological barrier at approximately 0.7 m before the 2.5 hour image duration was completed. In this case, the area of the vertical profile was saturated to the depth of the interpreted bedrock boundary in less time than 2.5 hours.

Vertical VS Lateral Flow

This analysis focuses on four flow types in which a spatial relationship on the plot can be derived from vertical and lateral flow. Vertical flow was utilized for hydraulic conductivity calculation. During wetting of the plot, areas within the wetting domain had begun to saturate at different rates. TERI data measured the amount of time elapsed for various locations within the wetting domain to infiltrate to an interpreted bedrock boundary, where vertical fluid migration was

heavily mitigated. Lateral flow was prevalent outside of the wetting domain on the transverse ERI lines. Some locations detected signal despite having no direct wetting. These locations also have sporadic vertical fluid migration intervals, different from those seen within the wetting domain. For example, (Figure 15) outside of the wetting domain exhibits peak conductivity values in sequential order that do not follow a successive saturation pattern such as (Figures 13 and 14) – both of which inside the wetting domain.

CONCLUSION

The TERI experiment indicates the ability to quantify the movement of water in the subsurface and to calculate the distribution of vertical hydraulic conductivity values in a heterogeneous soil using TERI profiles. This is important for managing riparian zones and other locations with significant macropore flow. TERI can help accurately locate areas of preferential flow caused by macropores, increasing the efficacy for placement and size of a riparian buffer. Results from this experiment are validated by ordinary soil moisture measurements and literature estimates. The hydraulic conductivity values for macropore flow compared to matrix flow in this research correspond to a similar ratio of hydraulic conductivity differences with macropore flow in coarse soil (Mallants et al. 1997).

The findings in this research also exhibit definitive lateral and vertical features on the TERI datasets. Lateral features indicate a fluid migration detected outside of the wetting domain in the plot, while vertical features were useful in calculating hydraulic conductivity. Both lateral and vertical TERI features warrant the discovery of four flow types found within the plot during

experimentation. The hydraulic conductivity calculations varied from 7 mm/hr to 1740 mm/hr. This vast difference in K values over a small area like the test plot supports the discovery of four flow types using this method.

REFERENCES

Acharya, B.S., Halihan, T., Zou, C.B., & Will, R.E. (2017). Vegetation controls on the spatio-temporal heterogeneity of deep moisture in the unsaturated zone: A hydrogeophysical evaluation. Scientific Reports, 7:1499, DOI: 10.1038/s41598-017-01662-y.

Beven, K., & Germann, P. (1982). Macropores and water flow in soils. Water Resour. Res., 18(5): 1311-1325. https://doi.org/10.1029/WR018i005p01311

Boyles, R. P., & Raman, S. (2003). Analysis of climate trends in North Carolina (1949–1998). Environ. Int., 29(2-3), 263-275. https://doi.org/10.1016/S0160-4120(02)00185-X

Cawthorn, J. W. (1970) Soil Survey, Wake County, North Carolina, US Soil Conserv. Service.

Christiansen, J. S., Thorsen, M., Clausen, T., Hansen, S., & Refsgaard, J. C. (2004). Modelling of macropore flow and transport processes at catchment scale. J. of Hydrol., 299(1-2), 136-158. https://doi.org/10.1016/j.jhydrol.2004.04.029

Cobb, W. B., & Hawker, H. W. (1918). Soil Survey of Payne County, Oklahoma, US Gov. Printing Office.

Dick, J., Terzlaff, D., Bradford, J., & Soulsby, C. (2018) Using repeat electrical resistivity surveys to assess heterogeneity in soil moisture dynamics under contrasting vegetation types, J Hydrology, 559, 684-697. https://doi.org/10.1016/j.jhydrol.2018.02.062

Edwards, W. M., Norton, L. D., & Redmond, C. E. (1988). Characterizing macropores that affect infiltration into nontilled soil. Soil Sci. Soc. of America J., 52(2), 483-487. https://doi.org/10.2136/sssaj1988.03615995005200020033x

Fox, G. A., Felice, R. G., Midgley, T. L., Wilson, G. V., and Al-Madhhachi, A. S. T., 2014, Laboratory soil piping and internal erosion experiments: evaluation of a soil piping model for low-compacted soils: Earth Surface Processes and Landforms, v. 39, no. 9, p. 1137-1145.

Fuchs, J. W., Fox, G. A., Storm, D. E., Penn, C. J., & Brown, G. O. (2009). Subsurface transport of phosphorus in riparian floodplains: Influence of preferential flow paths. J. Environ. Qual., 38(2), 473-484. https://doi.org/10.2134/jeq2008.0201

Guertault, L., Fox, G. A., Dowdy-Green, R., and Halihan, T. J. A., 2019, In-situ experiments and quantification of the influence of preferential subsurface flow on water and contaminant transfer through riparian buffers, v. 2019, p. H51E-04.

Guertault, L., Fox, G. A., Halihan, T., & Munoz-Carpena, R. (2021). Quantifying the importance of preferential flow in a riparian buffer. T. ASABE.

Griffiths, D.H. & Turnbull, J. (1985) A multi-electrode array for resistivity surveying, First Break, 3(7), https://doi.org/10.3997/1365-2397.1985013

Gunn, D., Chambers, J., Uhlemann, S., Wilkinson, P., Meldrum, P., Dijkstra, T., Haslam, E., Kirkham, M., Wragg, J., Holyoake, S. J. C., and Materials, B., 2015, Moisture monitoring in clay embankments using electrical resistivity tomography, v. 92, p. 82-94.

Halihan, T., Paxton, S., Graham, I., Fenstemaker, T., & Riley, M. (2005). Post-remediation evaluation of a LNAPL site using electrical resistivity imaging. J. of Environ. Monitoring, 7(4), 283-287. =-

Halihan, T., Miller, R. B., Correll, D., Heeren, D. M., & Fox, G. A. (2019). Field evidence of a natural capillary barrier in a gravel alluvial aquifer. Vadose Zone J., 18(1), 1-12. https://doi.org/10.2136/vzj2018.01.0008

Heeren, D. M., Fox, G. A., & Storm, D. E. (2015). Heterogeneity of infiltration rates in alluvial floodplains as measured with a berm infiltration technique. Trans. ASABE, 58(3), 733-745. https://doi.org/10.13031/trans.58.1105

Jarvis, N. J., 2007, A review of non-equilibrium water flow and solute transport in soil macropores: Principles, controlling factors and consequences for water quality, v. 58, no. 3, p. 523-546.

Jarvis, N. J., Jansson, P. E., Dik, P. E., & Messing, I. (1991). Modelling water and solute transport in macroporous soil. I. Model description and sensitivity analysis. J. of Soil Sc., 42(1), 59-70. https://doi.org/10.1111/j.1365-2389.1991.tb00091.x

Jarvis, N. J., & Larsson, M. (2001). Modeling macropore flow in soils: Field validation and use for management purposes. In Conceptutal Models of flow and transport in the factured vadose zone. Nat. Academics Press, Washington, D.C., p. 189-216.

Jung, Y., Ha, H., & Lee, Y. (2000). Application of electrical resistivity imaging techniques to civil and environmental problems. Geo-Denver 2000. In Use of Geophysical Methods in Construction. pp. 52-64. Denver, CO. https://doi.org/10.1061/40521(296)4

Koestel, J. K., Moeys, J., and Jarvis, N. J. (2012). Meta-analysis of the effects of soil properties, site factors and experimental conditions on solute transport. Hydrol. Earth Syst. Sci. 16, 1647-1665.

Lee, P., Smyth, C., & Boutin, S. (2004). Quantitative review of riparian buffer width guidelines from Canada and the United States. J. of Environ. Manag., 70(2), 165-180. https://doi.org/10.1016/j.jenvman.2003.11.009

Lim, Y. Y., & Miller, G. A. (2004). Wetting-induced compression of compacted Oklahoma soils. J of Geotechnical and Geoenvironmental Eng., 130(10), 1014-1023. https://doi.org/10.1061/(ASCE)1090-0241(2004)130:10(1014)

Loke, M.H., Acworth, I., & Dahlin, T (2003). A comparison of smooth and blocky inversion methods in 2D electrical imaging surveys, Explore. Geophysics, 34(3), 182-187.

Mallants, D., Mohanty, B. P., Vervoort, A., and Feyen, J., 1997, Spatial analysis of saturated hydraulic conductivity in a soil with macropores: Soil Technology, v. 10, no. 2, p. 115-131.

Menichino, G.T., Ward, A.S. & Hester, E.T. (2014) Macropores as preferential flow paths in meander bends, Hydrol. Process., 28, 482-495. http://doi.org/10.1002/hyp.9573

Minet, J., Wahyudi, A., Bogaert, P., Vanclooster, M., and Lambot, S. J. G., 2011, Mapping shallow soil moisture profiles at the field scale using full-waveform inversion of ground penetrating radar data, v. 161, no. 3-4, p. 225-237.

Mishra, V., Ellenburg, W. L., Al-Hamdan, O. Z., Bruce, J., and Cruise, J. F. J. E., 2015, Modeling soil moisture profiles in irrigated fields by the principle of maximum entropy, v. 17, no. 6, p. 4454-4484

Moysey, S. M., and Liu, Z., 2012, Can the onset of macropore flow be detected using electrical resistivity measurements?, v. 76, no. 1, p. 10-17.

Mullens, E. D., Shafer, M., & Hocker, J. (2013). Trends in heavy precipitation in the southern USA. Weather, 68(12), 311-316.

Orozco-Lopez, E., Muñoz-Carpena, R., Gao, B., & Fox, G. A. (2018). Riparian vadose zone preferential flow: Review of concepts, limitations, and perspectives. Vadose Zone J., 17, 180031. https://doi.org/10.2136/vzj2018.02.0031

Robinson, J.L., Slater, L.D., & Schäfer, K.V.R. (2012) Evidence for spatial variability in hydraulic redistribution within an oak–pine forest from resistivity imaging, J. Hydrol. 430-431: 69-79. https://doi.org/10.1016/j.jhydrol.2012.02.002

Sabbagh, G. J., Fox, G. A., Kamanzi, A., Roepke, B., & Tang, J. Z. (2009). Effectiveness of vegetative filter strips in reducing pesticide loading: Quantifying pesticide trapping efficiency. J. Environ. Qual., 38(2), 762-771. https://doi.org/10.2134/jeq2008.0266

Shanahan, P. W., Binley, A., Whalley, W. R., and Watts, C. W. J. S. S. S. o. A. J., 2015, The use of electromagnetic induction to monitor changes in soil moisture profiles beneath different wheat genotypes, v. 79, no. 2, p. 459-466.

Simunek, J., Jarvis, N. J., van Genuchten, M. Th., & Gardenas, A. (2003). Review and comparison of models for describing non-equilibrium and preferential flow and transport in the vadose zone. J. Hydrol. 272, 14-35.

Van Nostrand, R.G., & Cook, K.L. (1966) Interpretation of resistivity data, USGS Professional Paper 499, https://doi.org/10.3133/pp499

Sudicky, E. A. J. W. R. R., 1986, A natural gradient experiment on solute transport in a sand aquifer: Spatial variability of hydraulic conductivity and its role in the dispersion process, v. 22, no. 13, p. 2069-2082.

Van Nostrand, R.G., & Cook, K.L. (1966) Interpretation of resistivity data, USGS Professional Paper 499, https://doi.org/10.3133/pp499

Wehrspohn, R., Ozanam, F., and Chazalviel, J. N. J. J. o. T. E. S., 1999, Nano-and Macropore Formation in p-Type Silicon, v. 146, no. 9, p. 3309.

Weiler, M., & Naef, F. (2003). Simulating surface and subsurface initiation of macropore flow. J. of Hydrol., 273(1-4), 139-154. https://doi.org/10.1016/S0022-1694(02)00361-X

Weiler, M., & Naef, F. (2003). An experimental tracer study of the role of macropores in infiltration in grassland soils. Hydrol. Process., 17(2), 477-493. https://doi.org/10.1002/hyp.1136

Williams, M. R., King, K. W., Ford, W., Buda, A. R., & Kennedy, C. D. (2016). Effect of tillage on macropore flow and phosphorus transport to tile drains. Water Resour. Res., 52(4), 2868-2882 https://doi.org/10.1002/2015WR017650

Wilson, G., 2011, Understanding soil-pipe flow and its role in ephemeral gully erosion: Hydrological processes, v. 25, no. 15, p. 2354-2364.

Wilson, G. V., Wells, R., Kuhnle, R., Fox, G., and Nieber, J., 2018, Sediment detachment and transport processes associated with internal erosion of soil pipes: Earth Surface Processes and Landforms, v. 43, no. 1, p. 45-63

Zhang, X. C., & Nearing, M. A. (2005). Impact of climate change on soil erosion, runoff, and wheat productivity in central Oklahoma. Catena, 61(2-3), 185-195. https://doi.org/10.1016/j.catena.2005.03.009

Zhou, Q.Y., Shimada, J., & Sato, A. (2001) Three-dimensional spatial and temporal monitoring of soil water content using electrical resistivity tomography, Water Resour Res, 37(2), 273-285.

Zarroca, M., Linares, R., Velásquez-López, P. C., Roqué, C., & Rodríguez, R. (2015). Application of electrical resistivity imaging (ERI) to a tailings dam project for artisanal and small-scale gold mining in Zaruma-Portovelo, Ecuador. J. of Appl. Geophysics, 113, 103-113.

VITA

John Paul Hager

Candidate for the Degree of

Master of Science

Thesis: EVALUATING MACROPORE FLOW WITH ELECTRICAL RESISTIVITY IMAGING IN RIPARIAN AREAS

Major Field: Geology

Biographical:

Education:

Completed the requirements for the Master of Science in Geology at Oklahoma State University, Stillwater, Oklahoma in May, 2021.

Completed the requirements for the Bachelor of Science in your Geology at Western Michigan University, Kalamazoo, MI/USA in June, 2018.

Experience:

Field Technician: Aestus LLC, May 2019 – Present

Student Geologist: Michigan Geological Repository for Research and Education, September 2015 – June 2018

Professional Memberships:

AIPG, GSA, & ASABE